A. SPECIFIC AIMS – Project 1: Image Acquisition Calibration and Correction

Project 1 builds on the momentum developed during the first phase of the Morphometry BIRN (mBIRN) to standardize the multi-site structural MRI acquisition protocols and calibrate the image data in order to identify and minimize sources of image variance and distortion. In this renewal, we propose to move beyond the initial mBIRN objectives to incorporate the multi-site acquisition of a wider range of image data types in order to support the more sophisticated analyses envisioned by our clinical collaborators. This will be done using a two-staged approach:

- Stage I (years 1-3): we will focus on expanding calibration protocols that primarily support key clinical collaborators who work with Alzheimer Disease/Elderly Depression populations (ongoing and new collaborations including VETSA, and NIA Neuroimaging Initiative, see the Clinical Collaboration section). During Stage I we will also identify image modalities that we are not currently proposing to calibrate, but that will be necessary for supporting other brain diseases to be addressed in Stage II (e.g., Multiple Sclerosis and HIV (see Clinical Collaboration section, CHARTER grant)).
- Stage II (years 4-5): we will make available to the public the protocols developed in Stage I and we will expand our calibration efforts to support additional neuroimaging modalities that support clinical research other than AD and Depression as identified in Stage I. During Stage II we will also identify new collaborators who are studying non-brain diseases for which quantitative whole body structural imaging (e.g. DTI in heart) is of critical importance. The input from these new collaborators will be used to develop the strategies and prototype efforts to extend our image acquisition calibration and correction efforts beyond the brain.

This proposal focuses on the work plans for Stage I. Specifically, during Stage I of this renewal period, we will add the ability to operate on MR morphometry data collected on scanners of multiple manufacturers and field strengths (1.5T Siemens/GE/Picker/ Philips, 3.0T Siemens/GE, and 4.0T GE) whereas the original mBIRN efforts were focused on 1.5T Siemens/GE/Picker scanners. Similarly, we will add support for additional image acquisitions such as FSE (fast spin-echo), proton density (PD), T_2-weighted images and Fluid Attenuated Inversion Recovery (FLAIR) imaging. These new types of input image data provide a more complete picture of brain morphometry including both gray matter structures and white matter structure together with the ability to detect white matter abnormalities and lesions, which are co-morbid with morphometric changes in cortical and subcortical gray matter. Together these capabilities will facilitate precise, quantitative, platform independent, multi-site evaluation of normal and pathological structural imaging data. We will also develop the ability to support diffusion tensor imaging (DTI) in addition to continuing the improvements of T_1 weighted imaging that has been used to date. At the end of Stage I, we will have recommendations for T_1, T_2 and DTI protocols and procedure for minimizing sources of variability with these acquisition modalities. The protocols and correction methods will be made available to the clinical research community.

A unified approach will be used to address the calibration goals of both structural and diffusion MRI. First, using local expertise from the participating sites we will evaluate methods for image acquisition and correction at individual sites. Second, a common protocol for acquisition and correction methods will be tested across the participating sites, using traveling volunteers, to quantify reproducibility. The acquisition and correction methods that will be developed using the expertise from the participating sites are separated in two aims, one to address conventional T_1- and T_2-weighted structural MRI, and the other for diffusion-weighted MRI. Our aims are:

Aim 1: Develop methods to improve structural 3-D T_1- and Fast Spin Echo (FSE) based Proton Density (PD), T_2-weighted as well as Fluid Attenuated Inversion Recovery (FLAIR) weighted MRI acquisition protocols that maximize image quality, improve sensitivity, reduce noise and enable quantitative analysis across sites and instruments. For these structural MRI methods the goals are to:

1.1 Reduce spatial variation in RF-coil sensitivity due to B_1 field inhomogeneity
1.2 Reduce spatial distortion due to B_0 field inhomogeneity
1.3 Reduce signal changes and artifact due to head motion during scanning
1.4 Reduce gradient distortions, now extended to new vendors and scanner models
1.5 Continue with the calibration of T_1 acquisitions, extended to new vendors and multiple field strengths
1.6 Calibrate FSE-based PD, T_2-weighted and FLAIR acquisitions across sites, vendors, field strengths, protocols
1.7 Calibrate and model healthy and lesion brain tissue contrast (PD, T_1-weighted, T_2-weighted and FLAIR) as a function of field strength, scanner model, and pulse sequence

Aim 2: Develop improved diffusion MRI protocols and correction methods that minimize variability across

sites while optimizing image quality and accuracy. For diffusion MRI the goals are to:

   2.1 Characterize and correct for B_0 inhomogeneities in EPI- and Spiral-based DTI acquisitions
   2.2 Characterize reduce dependence on SNR, spatial resolution, b-value, and gradient encoding directions

B. BACKGROUND AND SIGNIFICANCE

   A major motivation for the mBIRN effort is the potential it promises for data mining and meta-analysis across imaging sites. However, precise, quantitative analysis and comparison of image data across sites is severely hampered by site-specific factors, such as scanner hardware and software versions, resulting in significant and systematic differences in imaging results at different sites, and across time at the same site.

B.1 Accuracy and reproducibility in multi-site T_1 and T_2 structural MRI

   Based on the high degree of anatomical detail available in typical MRI images, it is often assumed that the effects of geometric distortion and image artifacts are relatively minor. Consequently, corrections for such effects are very rarely incorporated into studies based on structural imaging data. However, the errors introduced by distortions and artifacts can in fact be quite large, especially relative to the subtle structural effects of interest in clinical studies, and may thus severely limit the accuracy and reproducibility of the results. Reproducibility of results across time is particularly important in longitudinal studies, where the goal is to identify subtle structural or functional changes that occur within individuals over time. Thus, reducing scan-rescan variability has a direct effect on statistical power of such studies. Absolute accuracy of the geometric models is particularly important when data are to be used for quantitative modeling (e.g., for morphometry), and when co-registering data across modalities (e.g., structural MRI with fMRI or diffusion MRI) or across field strengths (e.g., morphometry data from 3T and 1.5T). Integration of structural and fMRI data from various field strengths is essential for meaningful analysis and interpretation of the data collected by the FIRST BIRN testbed and the collaborative studies we support through that mechanism. Absolute accuracy is also essential when comparing or combing imaging data acquired at different sites or scanner models, as site-specific distortions and artifacts may introduce bias and erroneous results that are of the same or greater magnitude as the anatomical changes of interest. In order to maximize the accuracy and reproducibility of the geometric models constructed using our automated tools, and to maximize the value of the proposed multi-spectral statistical atlas, we propose to develop and apply procedures for characterizing and correcting the major sources of image distortion. Note that while the initial focus of the mBIRN testbed is on brain imaging, many of the methods for improved image acquisition and correction apply directly to other imaging applications. In fact, some of the issues, such as distortions due to gradient nonlinearities and B_0 inhomogeneities are even more pronounced for whole body imaging studies, in which the required field of view (FOV) is larger. We therefore anticipate that the technologies developed and validated in Stage I of this renewal will be important to the extension of the BIRN initiative beyond neuroimaging in Stage II.

B.1.1 Correction for spatial distortion due to B_0 field in-homogeneity

   A significant source of error in the reconstructed geometrical models of brain anatomy is spatial distortion due to inhomogeneities in the main magnetic field B_0, which can arise due to imperfect shimming, magnetic susceptibility effects and chemical shift. These effects can become particularly important for longitudinal studies in which different shim settings can result in substantial differential distortions between scan sessions. Although these distortions are most pronounced in functional imaging (or diffusion weighted imaging) using Echo Planar Imaging (EPI) sequences, the effects can be significant (on the order of several millimeters) even in conventional structural images. This is illustrated in **Figure B.1**, which shows close-ups of a coronal slice through the right temporal lobe of a subject, acquired with opposite readout directions (head-to-foot vs. foot-to-head). Note the compression / expansion of the gray matter around the ear canal (indicated by a red marker), making accurate surface reconstruction and gray/white segmentation very problematic in this region. Corrections for such distortions are rarely applied in functional or structural imaging studies. Here we propose to reduce B_0 inhomogeneity distortions through the use of two correction methods: a) MRI sequence optimization (multi-echo FLASH) and b) improved image reconstruction techniques (time domain reconstruction with alternating readout direction acquisitions). These correction methods will be described in Methods D.1.2.
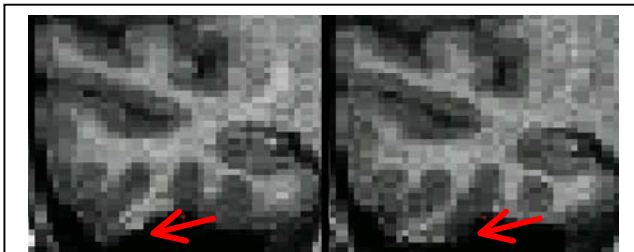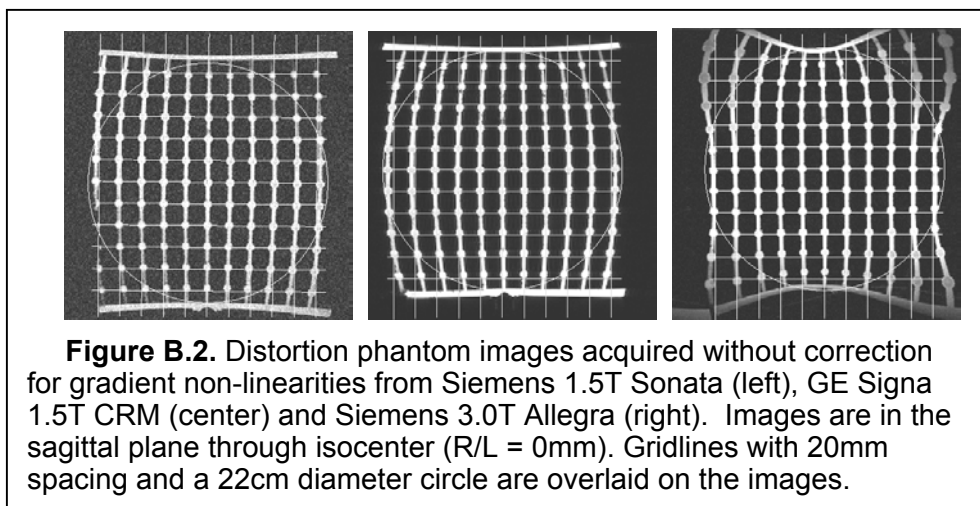

Figure B.1. Spatial distortion of structural MRI data due to magnetic susceptibility effects.

B.1.2 Correction for head motion during scanning

One of the main sources of artifacts in structural images is subject motion. While motion between scans and sessions can usually be corrected using standard motion correction algorithms (Woods, 1998), such corrections are typically associated with a certain loss of resolution, due to the interpolation required. Furthermore, such methods are entirely inappropriate for within-scan motion, which produces time-varying rotations and phase shifts in the Fourier domain (k-space). In order to reduce or eliminate artifacts caused by within-scan motion, we propose to implement a recently developed real-time motion correction approach, using so-called Cloverleaf Navigators, on multiple MR scanner platforms (See Methods D.1.3). We anticipate that this will significantly improve image quality and test-retest reproducibility, especially in patients with dementia or certain movement disorders. We anticipate that this method will also be applicable to imaging outside the head. This will be explored in Phase II of the renewal.

B.1.3 Correction for gradient distortions, extended to new vendors and scanner models

Another major source of error in structural and functional images is spatial distortion due to gradient nonlinearity (Wald, 2001). Accurate spatial co-registration between functional and structural data is essential for appropriate interpretation of functional imaging results, especially in studies of functional topography on the cortical surface (e.g., retinotopic mapping), where mis-registration of a few millimeters can result in significant errors. One cause of mis-registration is spatial distortion of the anatomical or functional images due to gradient nonlinearity; the deviation of the gradient field from an ideal linear function of position. This is particularly prominent on the latest generation of MRI systems that have been optimized for gradient strength and slew rate at the expense of gradient linearity. Although this improves magnetic susceptibility induced distortion in EPI, the gradient nonlinearity distorts the basic image coordinate system, affecting structural as well as functional images. For examples of such distortions, see **Figure B.2**, which shows standard structural images acquired on three different clinical MRI scanners, of a custom built cylindrical phantom containing a 3-D lattice of fluid-filled depressions. Note the difference in distortion patterns for dif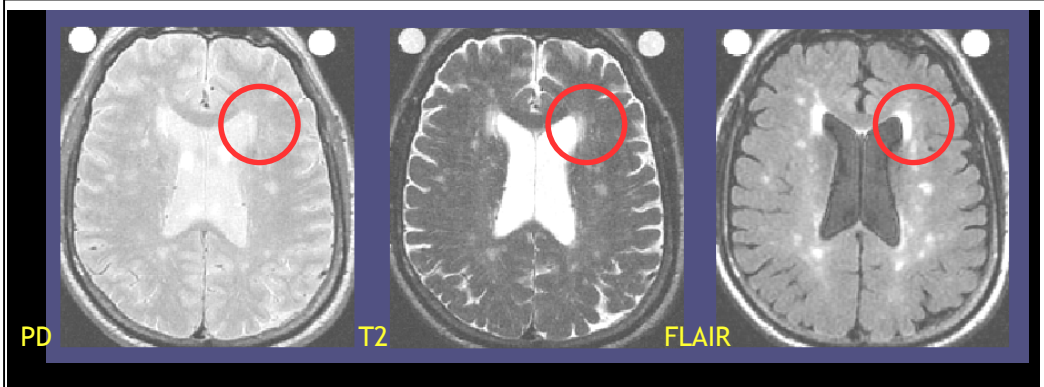ferent scanner models. As part of the proposed project, we intend to implement correction procedures for these distortions, using DICOM header information and a library of spherical harmonic coefficients specifying the characteristic distortion pattern for each scanner manufacturer and model. In the first funding cycle of the mBIRN grant we addressed the gradient distortion correction of the mBIRN sites, which were all 1.5T systems. This progress is reported in detail in C.1. In this renewal we will extend the work to higher field strengths (4T and 3T) in

Figure B.2. Distortion phantom images acquired without correction for gradient non-linearities from Siemens 1.5T Sonata (left), GE Signa 1.5T CRM (center) and Siemens 3.0T Allegra (right). Images are in the sagittal plane through isocenter (R/L = 0mm). Gridlines with 20mm spacing and a 22cm diameter circle are overlaid on the images.

order to support data integration with FIRST BIRN and with MRI systems used for diffusion MRI (See Methods D.1.4).

B.1.4 Calibration of FSE-based PD, T_2 and FLAIR weighted acquisitions across sites, vendors, field strengths, protocols

While T_1-weighted MRI acquisitions have been very useful for depiction of near-normal anatomy, other methods have been used to highlight brain abnormalities such as lesions and edema. Fast-spin-echo pulse sequences make it possible to obtain PD weighted and T_2-weighted images with a resolution comparable to that of T_1-weighted images that are in good registration in a reasonable imaging time on the order of 5 to 10 minutes. Also, such acquisitions can achieve higher contrast-to-noise ratios for proton density weighting than for spoiled gradient echo sequences that use a very small flip angle to get PD weighting. Finally, as illustrated in **Figure B.3**, FLAIR methods add the advantage of suppression of free water by using an inversion pulse and suitable timing resulting in a T_2-weighted image that is sensitive to elevated T_2 while eliminating free fluid such as CSF. This has been very valuable in the detection of peri-ventricular lesions. The approach has also been

shown to be very useful in the detection of the vascular lesions (unidentified bright objects- UBOs) associated with depression, vascular dementia, multiple sclerosis or even the normal aging brain. The FSE sequences have the additional advantages that they are less sensitive to magnetic field inhomogeneity and susceptibility differences than gradient echo methods although they do suffer similar sensitivity to gradient field nonlinearity and motion. The concerns for these approaches for multi-site studies are the extent to which manufacturer differences in pulse sequence design

Figure B.3. Illustration of the different sensitivities of PD, T2 and FLAIR weighted images to detect white matter lesions

require different sets of pulse sequence parameters for optimization; the degree to which tissue contrast changes with field strength; the extent to which various artifacts due to, for example, RF field inhomogeneity, flow or RF pulse design compromise across site results; and the extent to which RF pulse power deposition limits restrict performance at higher magnetic field strengths. These concerns motivate the proposed Methods outlined in D.1.2 and D.1.5.

B.2 Accuracy and reproducibility in multi-site diffusion MRI

DTI is a relatively new imaging modality, which provides unique information about microstructure of fibrous tissues such as cerebral white matter (Moseley, 1990; Basser, 1994; Makris, 1997). The raw data from a diffusion imaging experiment consists of a series of diffusion-weighted images (DWIs), from which the diffusion tensor and associated vector and scalar maps can be calculated. This is similar to the relationship between T_2-weighted images and a calculated T_2 map. However, contrary to the T_2 structural imaging, in which signal intensity is investigated as a function of scalar parameter (echo time), in diffusion tensor imaging, the signal is interrogated as a function of the diffusion gradient (**G**), which is a vector quantity. The relationship between diffusion-weighting and signal intensity is given by the following equation:

$$\ln\left[\frac{S}{S_0}\right] = -\int_0^t \gamma^2 \left[\int_0^{t'}\overline{\mathbf{G}(t'')}dt''\right] \bullet \overline{\overline{\mathbf{D}}} \bullet \left[\int_0^{t'}\overline{\mathbf{G}(t'')}dt''\right]dt'$$

where **D** is 3x3 diffusion tensor,**G** is the time course of the applied diffusion gradient (Basser, 1994).

Compared to conventional structural imaging, diffusion imaging has more freedom in the parameter choice, which can be a source of variability in experimental results. In addition to the imaging parameters, DTI has a number of unique sources of experimental variability. These include (**Figure B.4**):

Scanner specifications: Diffusion-weighting requires high-performance magnetic field gradient systems. Because of current active device development, available gradient strength, slew rate, linearity, and the amount of Eddy current distortions could also be highly variable across sites. These could be sources of poor across-institution reproducibility.
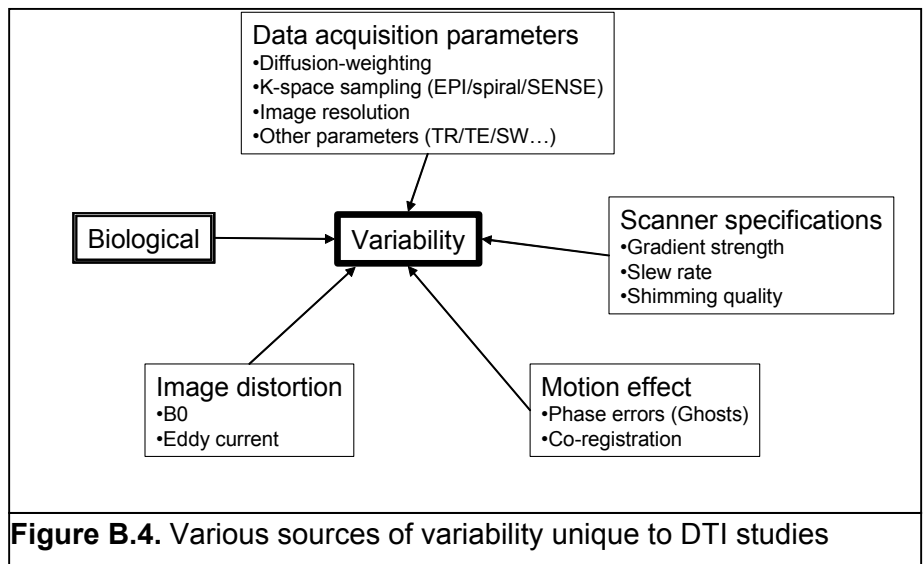
Figure B.4. Various sources of variability unique to DTI studies

Motion effects: DTI is a highly motion-sensitive MRI technique. The motion sensitivity is due to two factors. First, tensor calculations require precise co-registration of individual DWIs, which is sensitive to subject motion. More importantly, subject motion introduces phase errors under applied diffusion gradient, which leads to image artifacts.

Image distortion: Currently single-shot imaging is widely used for DTI to reduce the phase errors due to subject motion. However, single-shot imaging techniques are highly sensitive to B_0 field inhomogeneity, which leads to image distortion. In addition, the applied diffusion gradients induce Eddy currents in the MR bore and the supporting electronics. The induced Eddy currents generate magnetic fields that interfere with the image-encoding gradients, leading to image distortions. While all of the diffusion sampling directions suffer from the amount of the B_0-related distortion, the amount and nature of the Eddy current-related distortion varies for each diffusion sampling direction.

In order to sensitively and specifically investigate biological variability, the above-mentioned sources of variability must be kept constant. Using the same imaging protocols as much as possible within an institute can reduce the variability. However, for the across-institution variability, it is often impossible to employ the same protocols due to differences in pulse programs, scanner specifications, and availability of post-processing methods.

To facilitate inter-institutional data compatibility it is important to characterize these sources of variability and optimize the technology that is least affected by the variability. In this round of proposal, we will concentrate on the following two issues with highest priority. First, we will study several sources of variability, which are known to affect DTI results. These include various data acquisition parameters and image distortion (see **Figure B.4**). Second, we will perform initial measurement of intra- and inter-institutional variability of DTI measurements as described in the Method section. In this effort, all scans will be performed on the same subject and follow a strict common protocol to minimize the contribution of "Data Acquisition Parameters" in **Figure B.4**. In addition, "Image Distortion" contribution will be measured and minimized by using a distortion correction tool. This will provide information about the influence of "Scanner Specifications" and "Motion Effects".

C. PROGRESS REPORT AND PRELIMINARY DATA

During the initial phase of this research grant, we have made significant progress towards standardizing and calibrating 3D structural 1.5T MRI acquisition protocols as well as optimizing automated brain tissue segmentation methods that exploit multi-spectral MRI contrast information. These results have been presented in abstract form at international conferences (Society for Neurosciences 2003, Human Brain Mapping 2003 and 2004, and International Society for Magnetic Resonance in Medicine 2004, {see Appendix). And, although it was not in our initial cycle aims, we have also made progress in optimizing diffusion acquisition protocols, which are relevant for the new aims proposed in this renewal. Major developments include 1) methods for reducing test-retest variability of multi-spectral structural MRI, 2) methods for using multi-spectral MRI information to more accurately segment healthy and disease brain tissue and 3) methods for improving the geometric accuracy of diffusion MRI.

C.1 Evaluating effects of gradient distortion correction on image reproducibility

As one step toward our goal to standardize and calibrate image acquisition protocols to facilitate precise, quantitative evaluation of imaging data using
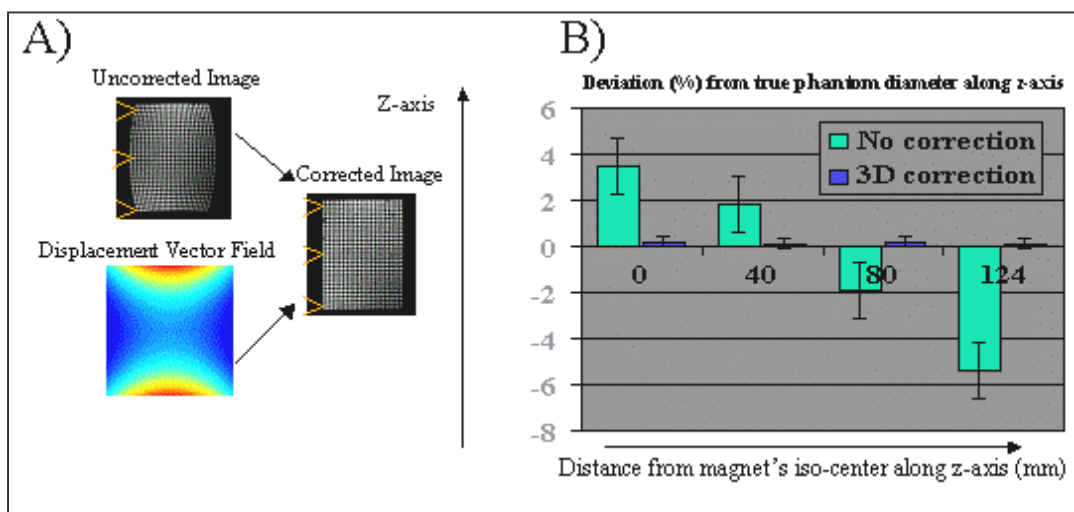

Figure C.1. Multi-site gradient distortion correction evaluation using a phantom. A) Schematic representation of the distortion correction process. B) Variability of phantom measures across sites, with and without gradient distortion correction, as a function of the distance from magnet's iso-center along the z-axis (mm).

segmentation/ morphometry tools, minimizing dependence on site-specific factors, we assessed the effect of correcting for gradient non-linearities. With sufficient knowledge of the physical arrangement of the windings of the gradient coils, the true gradients can be computed using a Fourier-Legendre basis set. The coefficients of such an expansion can typically be obtained from the computer-aided manufacturing (CAM) program used to design the MR scanner. With such knowledge, one can compute the true and ideal gradients for each point in space, and hence design a procedure to remove the warping induced by the departures from linearity (assuming the warping is invertible). This amounts to computing displacement vector- and density correction (Jacobian) maps, the application of which to the original image results in the desired unwarped image. To pursue this goal we performed a study to characterize and correct the image distortions from the partner sites in which we implemented a common structural acquisition protocol and acquired inert and human phantom data from the participating sites and made within and across site reproducibility assessments. These results are described below:

Validation of gradient distortion correction: phantom study

Although distortions in MRI can arise from several factors, the most prominent factor in structural MRI is gradient nonlinearities. While in principle, the gradient distortion is addressable in manufacturer-supplied post-processing software, the gradient un-warping option available on most MR systems tends to exacerbate the miss-registration of 2D and 3D images, as conventional 2D images are usually corrected only in-plane, if at all. To quantitatively characterize the extent of this warping, images of a cylindrical phantom were collected from 4 commercial whole body scanners used for functional and structural studies amongst the BIRN sites: General Electric Signa CVi/NVi 1.5T at Duke and BWH (CRM gradients with max strength, slew rate = 40mT/m, 150T/m/s), the same vendor but different gradients for UCSD (22mT/m, 120mT/m/ms), and Siemens Medical Systems Magnetom Sonata 1.5T from MGH (Sonata gradients, 40mT/m, 200T/m/s). The phantom (250 mm diameter x 220mm) was constructed for this purpose from plastic plates with 10mm diameter fluid filled spherical depressions spaced on an even 20 +/-0.05 mm grid. First a displacement vector map was calculated using the spherical harmonic coefficients from the vendor's true gradients and second, the displacement map

was applied to the original image (**Fig. C.1**). An image intensity correction is necessary (Jacobian correction, color map in **Fig. C.1**) to account for the resampling of the voxels into the corrected volume. The uncorrected distortions are relatively large and differ significantly between systems, as can be seen in the results from **Fig. C.1**. Measurement of the phantom diameter at the isocenter, from sagittal images (which show the strongest distortions), showed that the uncorrected images were on average 5.4+−2% smaller than the true diameter at the edges of the phantom. The error corresponds to the variability of the estimates across sites. The same estimations on the corrected
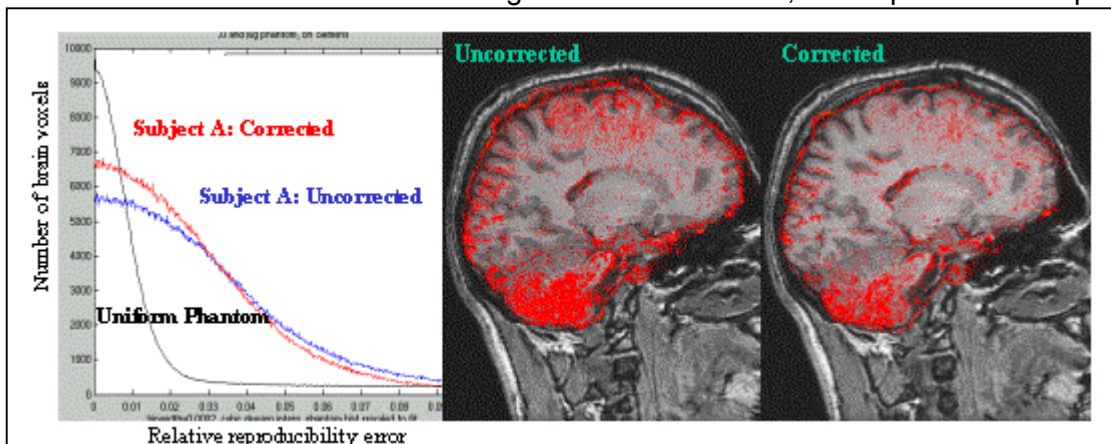
Figure C.2. Single subject, test-retest within site image intensity reproducibility.
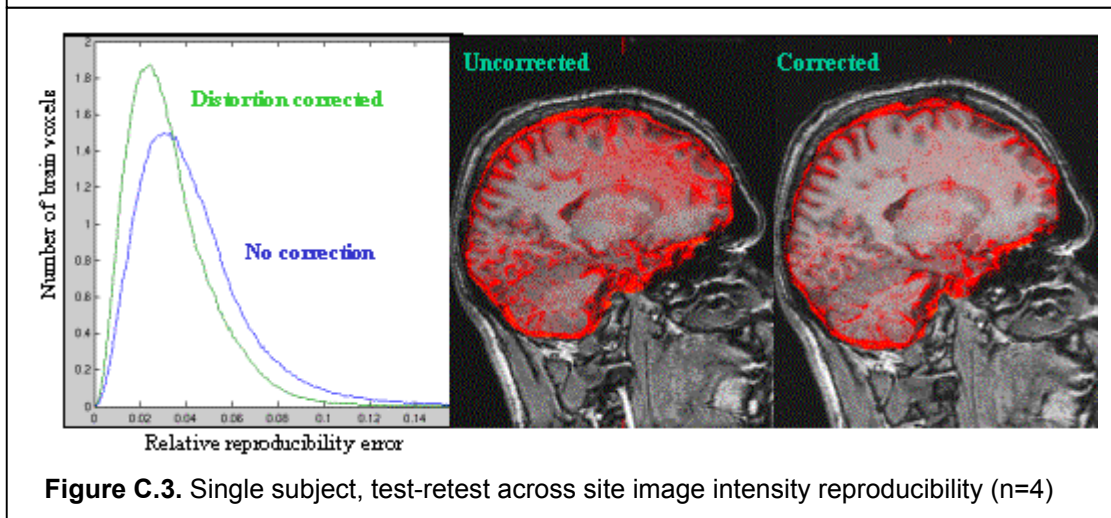
Figure C.3. Single subject, test-retest across site image intensity reproducibility (n=4)

images showed that the deviation from the true diameter was 0.5+-0.08%. The reduction of site-specific distortion effects due to gradient nonlinearities has the potential for improving the accuracy of morphometric analysis in longitudinal and multi-site imaging studies.

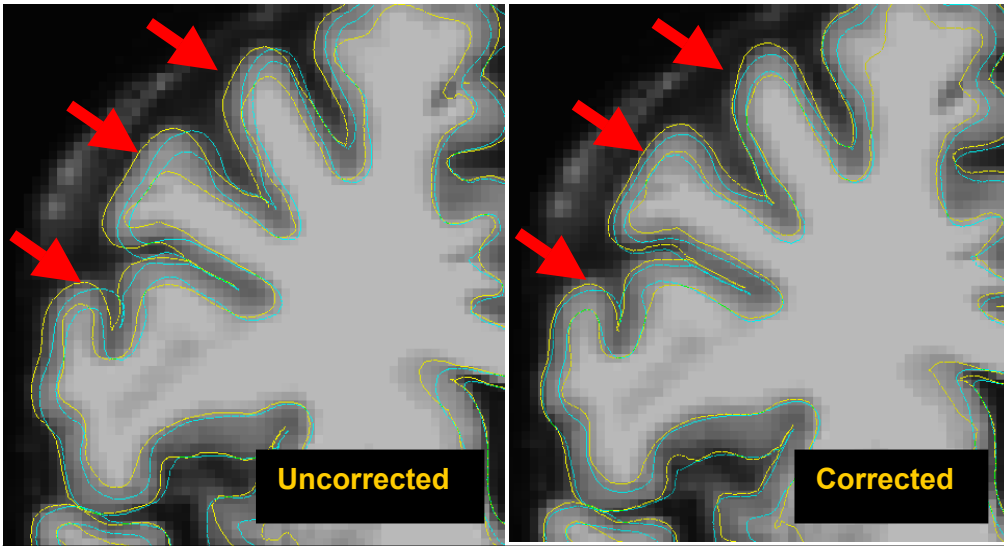Gradient distortion correction: Reproducibility effects in human data

After testing the correction algorithm with phantom data, the next planned step was to assess the impact of the gradient correction algorithm on site specific and across-site reproducibility of human structural MR data. We used four metrics to characterize image reproducibility: i) image intensity, ii) alignment of cortical surfaces, iii) volumes of subcortical structures and iv) cortical thickness (the subcortical and thickness estimates were obtained using Freesurfer software, discussed in detail in Project 2). Each of these metrics was measured from co-registered test-retest data, with and without distortion correction. To acquire the imaging data we first implemented a common structural MRI acquisition protocol across the mBIRN partner sites that allows for estimation of tissue parameters in a site-independent manner. This endeavor, our first experience with enforcing matching acquisition parameters across sites and platforms was successful in achieving the required consistency in the images. The calibration protocol consisted of four structural scans: 3D Sagittal FLASH/SPGR, TR/TE=20ms/6ms, 256x192, slice thickness=1.5mm, flip angles 30^0, 20^0, 5^0, 3^0, approximately 8 minutes per flip angle. Human test-retest scanning sessions (the whole protocol twice) were acquired across 5 sites on 6 healthy volunteers within a year. The reproducibility results obtained for the four metrics are described below.

Image intensity reproducibility: Gradient distortion correction is expected to affect image intensity reproducibility because distortions will affect voxel size. Image intensity variability was interrogated in two ways, by plotting a histogram of the relative reproducibility test-retest error distribution, and by inspection of color overlay maps, to evaluate the spatial distribution of the voxels with greater relative error. Figures C.2 and C.3 show sample variability histogram and variability map results from a single subject, within-site and across-site respectively. The color maps show voxels with relative error values greater than 8% (in red) overlaid on a representative anatomical gray scale image. As can be easily seen in the histograms of Figure C.3, the image intensity variability distribution shifts towards a lower mean when distortion correction is applied. In other words, the error is reduced and thus reproducibility is improved. Kolmogorov Smirnov tests showed that, both for within and across site comparisons (4 sites, 5 subjects), the means of the distortion corrected histograms were always significantly smaller then the means of the uncorrected data (Table C.1). As expected, the effects of the correction are strongest in across-site comparisons. However, these results show that the distortion correction does not correct for all the sources of image intensity variability (see also variability maps in Figures C.2 and C.3). Preliminary results (discussed in Section D) suggest that low-frequency image intensity variations produced by inhomogeneities of the B_1 RF pulses are an important source of image intensity variance.

Table C.1: Image intensity reproducibility results

GROUP RESULTS	Mean intensity reproducibility variance (no correction)	Average improvement of histogram mean (KS test, p<0.001)
Within-Site	4.4%	3.5%
Across-Site	8.8%	12.4%

Brain surface alignment reproducibility: The improvement in alignment reproducibility can be seen in **Figure C.4**, which shows the cortical surfaces (gray-pial and gray-white boundaries calculated using Freesurfer) from the same subject scanned at two different sites, and co-registered using one of the sites as reference. The colored surface contours are overlaid on the FLASH 30 of the reference site, yellow for the contours of the reference image and turquoise for the other site. As can be seen, the surface contours of the two scans are much better aligned when the data has been distortion corrected. *Note that in the absence of such corrections, it would be very difficult to distinguish true anatomical changes associated with disease from distortions caused by gradient nonlinearities and imperfect repositioning of the subject across scanning sessions or from changes due to changes in scanner hardware over time.* This is of particular importance in longitudinal studies looking for subtle anatomical changes over time (e.g., the ADNI collaborating project).
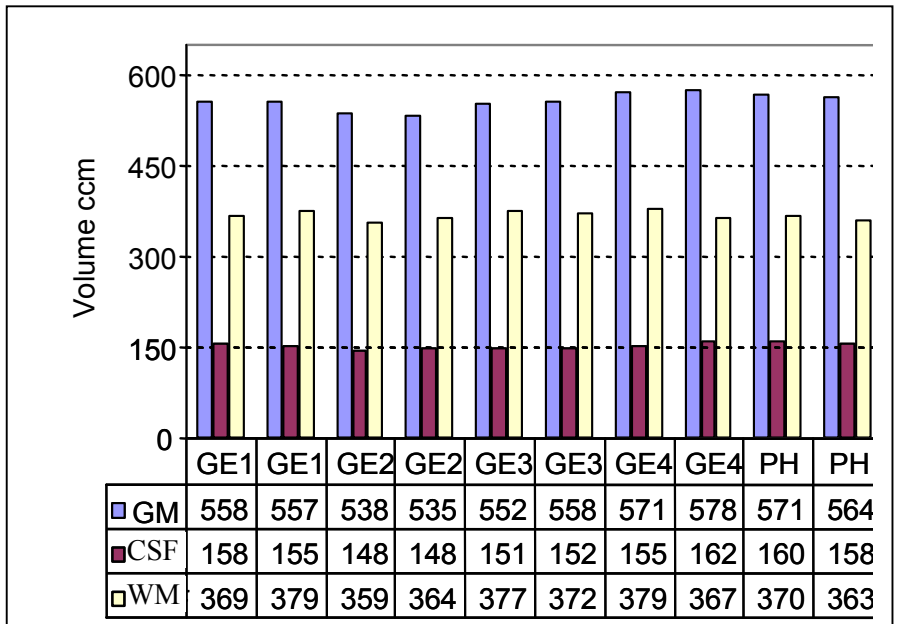
Figure C.4 Cortical boundaries of the same subject scanned at two different sites, with no distortion correction (left) and with distortion correction (right).

C.2 Evaluating variability in multiple sites using multiple contrast data

Data was gathered at five different 1.5T sites (four GE Signa systems and 1 Philips Gyroscan) with a single subject to evaluate the possible scanner-to-scanner differences for multi-contrast data. T_1, T_2 and proton density weighted scans were acquired twice on each scanner (consecutive days). The images were used in an automated image segmentation program to calculate the volume of gray, white and CSF regions (Styner, 2002). **Figure C.5** shows that the data is more reproducible within a given site as compared to up to 10% differences between sites. Thus it is likely that geometric calibration data from different sites will be as important in multi-contrast studies as it is in the T_1-weighted studies.

Using rule-based analysis with multiple contrasts to identify lesions

One approach to lesion identification is to consider them to be outliers in the distributions of image intensity as compared to normal brain tissue. This approach has been successfully used for detection of multiple sclerosis lesions in proton density and T_2-weighted images by implementing a simple rule that lesions are brighter than gray matter in both contrasts, are in white matter and are brighter than the tissue in which they are sampled using a criterion that the Mahalanobis distance (distance from the mean in standard deviation units) is greater than 3. The vascular lesions associated with aging and depression are brighter than surrounding white matter, but have an intensity that is similar to gray matter. Thus their identification is considerably simplified with the addition of other contrasts such as a FLAIR imaging channel. **Figure C.6** shows an example in which four different contrasts are used (PD, T_2, T_1 and FLAIR weighting) to detect white matter lesions.

	GE1	GE1	GE2	GE2	GE3	GE3	GE4	GE4	PH	PH
GM	558	557	538	535	552	558	571	578	571	564
CSF	158	155	148	148	151	152	155	162	160	158
WM	369	379	359	364	377	372	379	367	370	363

Figure C.5. Chart showing the comparison of volumes of gray, white matter and CSF in a single volunteer measured multiple times on several different 1.5T MRI systems (4 GE and 1 Philips) using PD, T2 and T1 weighted images and an automated, atlas driven image segmentation program.
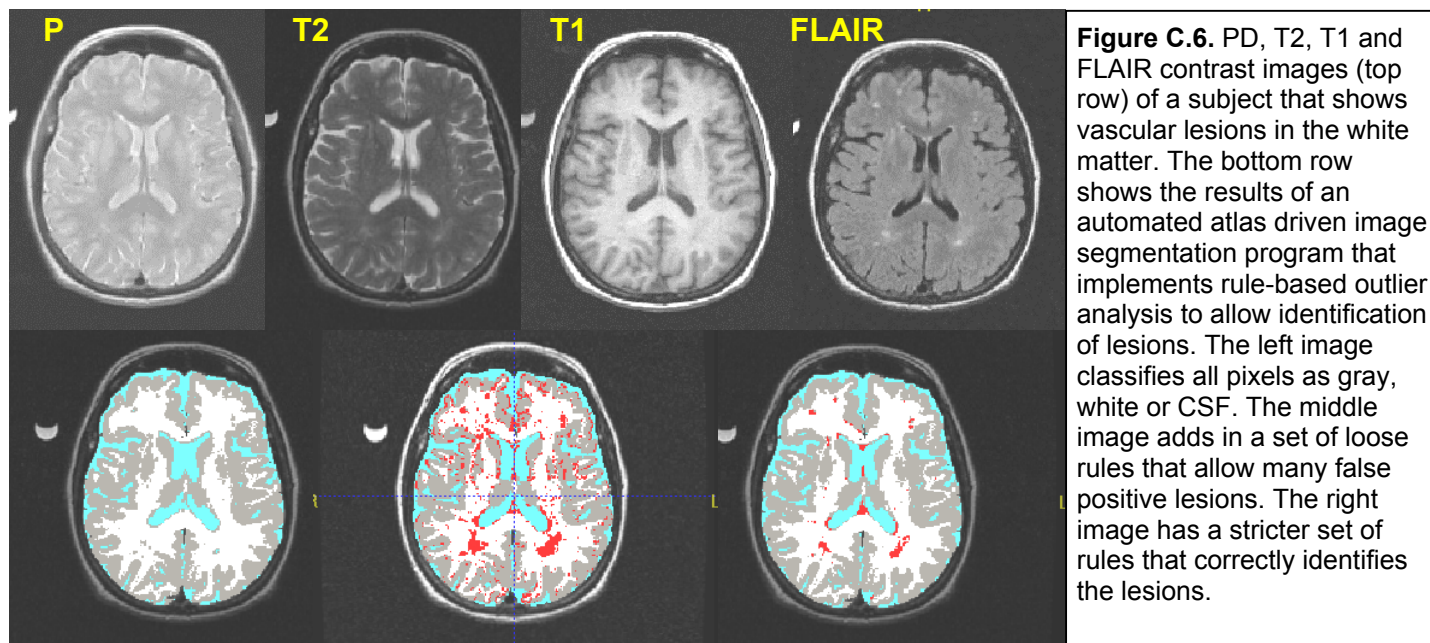
Clearly, the lesions show up well in the FLAIR channel and the T_2-weighted channel but are better distinguished from CSF in the FLAIR channel. The segmentations show the difference between not segmenting the lesions (which makes them show up as gray matter) or by using simple or complex rules to

define the lesions. While this rule tuning process requires considerable up-front effort, the result is an automated method that self adjusts to individual intensity changes.

Figure C.6. PD, T2, T1 and FLAIR contrast images (top row) of a subject that shows vascular lesions in the white matter. The bottom row shows the results of an automated atlas driven image segmentation program that implements rule-based outlier analysis to allow identification of lesions. The left image classifies all pixels as gray, white or CSF. The middle image adds in a set of loose rules that allow many false positive lesions. The right image has a stricter set of rules that correctly identifies the lesions.

## C.3 Improving geometric accuracy in diffusion MRI

The common multi-directional DTI acquisition scheme is based on the hypothesis that diffusion process can be treated mathematically as a tensor. The ADC (Apparent Diffusion Coefficient) and measures of anisotropy such as FA (Fractional Anisotropy) are determined from the diffusion tensor measured within each voxel. Fiber tracts are then generated from the FA between voxels. In standard DTI, a minimum of 6 non-coplanar directions is needed to determine the diffusion tensor. To achieve time efficiency such that the total acquisition time could be well tolerated by most human subjects, and to reduce the effects of subject motion, fast imaging techniques such as EPI or spiral are typically employed. Thus, the DTI images at present time suffer from common spatial distortions in EPI and spiral images, and additional diffusion-direction dependent distortions unique to DTI acquisition. Obviously, any global or individual spatial distortions within these diffusion-weighted images could affect the spatial accuracy of the ADC, FA and fiber maps. Our main goal for this sub-aim is then to allow reliable and efficient DTI acquisition while minimizing spatial distortions, as given in more detail in **Section D**. Precise spatial co-registration between these output images based on DTI acquisition and the high-resolution anatomical images could then be achieved. In this section two approaches and preliminary data are described for distortion reductions: use of main magnetic field maps (currently being developed at Duke) and time domain reconstruction (currently being developed at MGH). In the **Section D** we describe how these and other methods will be further tested and be shared with BIRN to characterize image reproducibility and accuracy as a function of parameters including field strength, vendor, acquisition sequence, sequence parameters.

C.3.1 Distortion reduction through field maps: EPI and Spiral acquisitions (Duke)

Since DTI images can be acquired using either EPI or spiral acquisitions, we organize our preliminary results for both the EPI and spiral images as they have different distortion characteristics. The main source of the spatial distortions arise from the field inhomogeneity under long readout times common to EPI and spiral acquisitions. However, due to the respective k-space sampling differences, EPI images suffer primarily from spatial displacement (geometric distortion) while spiral images are subject to spatial blurring. Nevertheless, both distortions will lead to spatial miss-registration to the high-resolution anatomical images, which must be reduced.

From the MR signal equation, it can be readily derived that when the field is homogeneous, the term ΔBo is zero and no distortions should occur if the gradient waveforms are faithfully generated. In the presence of a non-zero ΔBo, however, distortion will occur. Correction of this type of distortions thus requires information on ΔBo. In our preliminary work, we have implemented a method that uses the last two-phase images in the EPI time course as the seed images to measure a map of ΔBo. This method is quite robust if a reasonably

accurate field map is obtained. The image shown in **Figure C.7** (a) is a distorted image, which can be corrected to the form of image (c) by shifting the pixels back along the phase-encoding direction. However, there are concerns in that since the absolute field variation could be quite large, especially at high field scanners, the field map obtained using the current method may not be adequate as it may itself be distorted. Thus more refined methodology to ensure distortion-free field map is needed, more details will be given in **Section D**.


(a) **(b)** **(c)**
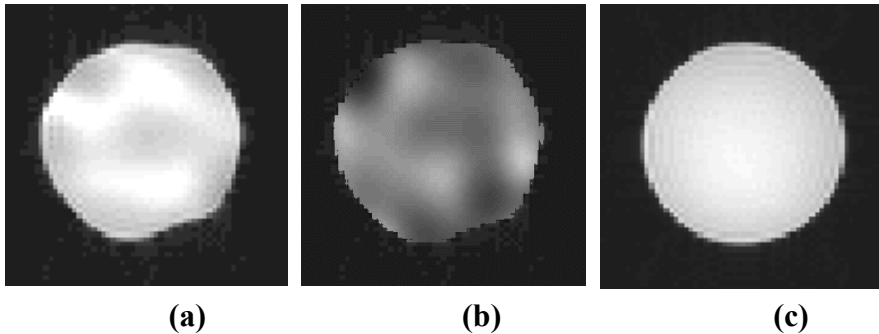
Figure C.7 (a) EPI images with inhomogeneity induced geometric distortions, (b) magnetic field map and (c) undistorted image.

While the geometric distortions in EPI k-space data are relatively straightforward to identify and correct, they are somewhat difficult if the k-space data is sampled in non-Cartesian coordinates, such as in the case of spiral imaging. Non-Cartesian measurements require re-gridding onto Cartesian coordinates, which involves applying a weighting function and spatial re-sampling. As a result, inhomogeneous magnetic fields and imperfect gradient systems are manifest as blurring artifacts. Different approaches are thus needed to address these artifacts as they specifically occur in spiral imaging.

Because long readout time would amplify this blurring effect, one method is to use interleaved spirals to reduce the readout time and hence the blurring artifact. This method, however, may not be practical in the case of single shot acquisitions commonly used for DTI acquisitions. Similar to the EPI correction scheme, a method that utilizes the Bo field map was implemented. In this implementation, a set of images reconstructed from a number of different frequencies was created by multiplying the k-space data by a complex exponential determined by a frequency shift. For each pixel in the final image, the field map was used to choose pixels from the appropriate frequency image. To demonstrate the effectiveness of the de-blurring effect, we used perfusion images from the flow-sensitive alternating inversion recovery (FAIR) preparation shown in **Figure C.8**. The image on the left was not reconstructed by using the multi-frequency decomposition, and the image on the right was. The effect of off-resonance related blurring was much reduced as indicated
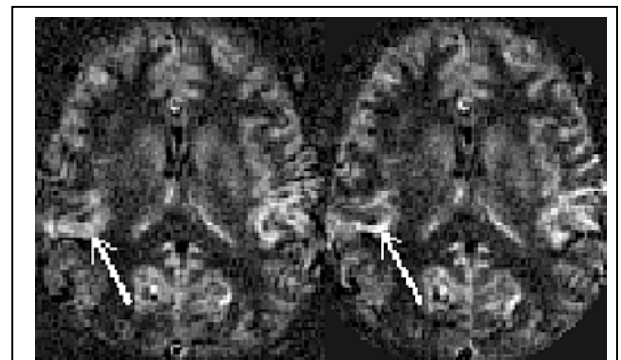
Figure C.8. The off-resonance correction using the technique described by Noll is illustrated. A field map was constructed from two images acquired at different echo times and an offset frequency was calculated for each pixel.
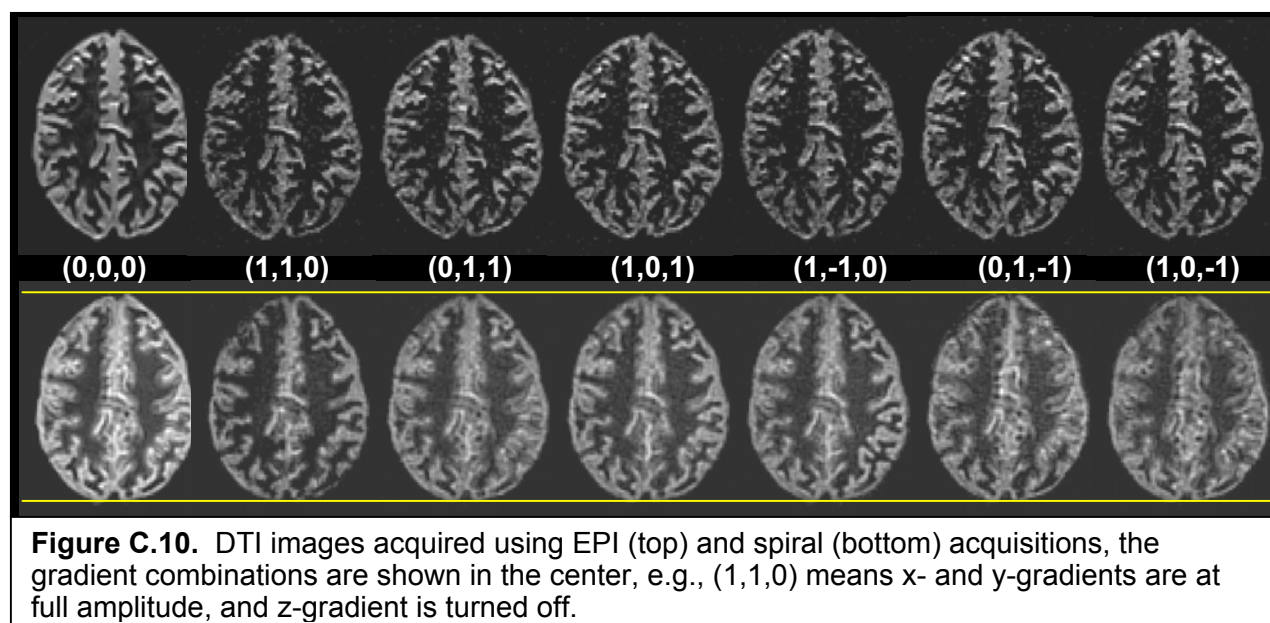
by the arrow. We used a perfusion image as an example here not only because it is easy to see the well-resolved vessels using the de-blurring technique, but also because of its potential application in fMRI as a valuable alternative to the BOLD methods. Other than the demonstration presented here, we will discuss the plan to develop perfusion imaging in **Section D**.

Spiral imaging typically applies both gradients simultaneously at a maximum slew rate or at maximum gradient strength during the entire readout time to improve the imaging efficiency. However, producing these time varying waveforms requires sufficient bandwidth of the gradient amplifier. Eddy currents related to these rapidly varying waveforms can distort the gradient fields and hence the spins being imaged. A method for measuring the actual

interleaf spiral.

gradient waveforms produced by the scanner hardware was developed and used by the applicants to correct images produced by scanners with imperfect hardware. **Figure C.9** shows the improvement of such a procedure. The effectiveness of this method is especially encouraging for DTI applications since large diffusion-weighting gradients are often employed and artifacts arising from eddy currents can be severe.

Preliminary DTI results using EPI and spiral acquisitions were also obtained. As mentioned earlier, in addition to the Bo inhomogeneity induced spatial distortions, additional diffusion-weighting direction-dependent distortions were apparent. **Figure C.10** illustrates diffusion-weighted images based on EPI (top) and spiral (bottom) acquisitions under various diffusion-weighting gradient combinations for a typical DTI acquisition. Significant spatial displacements of different magnitude across images along the phase-encoding anterior/posterior direction (shown as the non-continuous yellow edges across all seven images) are seen in EPI acquisitions, and direction-dependent spatial blurs are seen in spiral acquisitions. To correct for these direction-dependent spatial distortions, the conventional approach of acquiring one magnetic field map needs to be refined to correct for both the Bo inhomogeneity and gradient imperfections along different axes.

Figure C.10. DTI images acquired using EPI (top) and spiral (bottom) acquisitions, the gradient combinations are shown in the center, e.g., (1,1,0) means x- and y-gradients are at full amplitude, and z-gradient is turned off.

D. RESEARCH DESIGN AND METHODS

For the next phase of the mBIRN test bed work, we propose to provide critical advances that will increase the sensitivity and specificity of multi-site morphometric analyses. These advances are the characterization of acquisition protocols and data correction methods to improve sensitivity and reproducibility of multi-site 1) T_1-, PD-, and T_2–weighted structural MRI, and 2) diffusion MRI. It is expected that these advances will facilitate not only the BIRN projects, but also the work of other research groups conducting multi-site, quantitative structural MR studies. Importantly, the mBIRN efforts to provide recommendations for optimal scan acquisition parameters and correction methods will encompass the range of commonly employed image acquisition protocols. We chose this approach, rather than adopting a single "BIRN-mandated" protocol, because it will greatly increase the proportion of the biomedical imaging community who could benefit from our work. Further, while all our initial efforts in the first years of the study are focused on optimizing and correcting brain image data, the same methods and procedures can and will be adapted to support quantitative morphometric analysis as required to address biomedical investigation of a broader spectrum of disorders as described in the Clinical Collaboration section.

D.1 Coordination of multi-site calibration efforts

A Morphometry Calibration Working Group has been established. This Working Group includes Anders Dale and Larry Frank (UCSD), Jorge Jovicich and David Tuch (MGH), Allen Song and James MacFall (Duke), and Susumo Mori (JHU). The Morphometry Calibration Working Group will work closely with the other mBIRN sites by regular communications with their leadership (Steve Pieper at BWH, Randy Buckner at WashU, Arthur Toga at UCLA, Jessica Turner at UCI). The Morphometry Calibration Working Group will meet by

teleconference, email, or both at least once a month throughout the project to review progress, identify problem areas, and arrive at appropriate solutions.

For both structural and diffusion MRI, the calibration goals are:

1) Characterization of the effects of different protocols, scan parameters and systems' effects on reproducibility and accuracy of structural and diffusion MRI data
2) Test correction methods to maximize reproducibility and accuracy
3) Optimization of techniques to minimize cross-platform variability and validation of the developed standard multi-site protocols and correction methods

Given the unique expertise of each site, we propose the following strategy to maximize the efficiency in achieving our common goal. The initial work, as outlined in the subsequent sections, will be done using both appropriate phantoms and healthy human subjects studied at a subset of the sites. Based on individual expertise, specific members of the Morphometry Calibration Working Group will be responsible for implementing the first two steps (characterization and correction). For example, the UCSD and MGH group will take the lead on further improvements of 3-D T_1-weighted structural sequences, the Duke group will lead the characterization and optimization of FSE-based T_2- and PD-weighted sequences, the MGH, UCSD and JHU groups will lead the development and optimization of EPI-based DTI methods, and the Duke group will focus on Spiral-based DTI acquisitions and corrections. Once these first two steps are completed at the development sites, the algorithms/software will be shared among all mBIRN sites and any adaptations required to make them site independent will be made. The final step of minimizing cross-platform variability and validation of the developed standard multi-site protocols and correction methods will be coordinated by MGH and UCSD with support from all participating sites using cohorts of traveling human subject volunteers. We expect to be able to perform the data acquisition part of this third step in a coordinated fashion in a single cohort of 8 subjects for the T_1/T_2/PD structural MRI, and DTI sequences by the end of the first year. Section E. provides the details of subject recruitment, characterization and remuneration.

This sequence of steps will be repeated as necessary over the funding period to accommodate any hardware or software upgrades, advancements in image acquisition methods made by participating sites with co-located P41 projects, and requirements of new clinical collaborations at existing sites. An example of the latter case is described in Section D.1.5; our planned method for performing the optimization of T_2 scans in a population of elderly depressed subjects with known vascular lesions. This effort is critical to validate our proposed methods in populations with known pathophysiology that is detectable by morphometric analysis. The need to perform the cross scan platform, cross-field strength reliability study is well justified in this population.   However, to minimize the risk and burden on the human volunteer patients, this data will be collected at a single site (Duke) that has access to all the listed scanners. The Morphometry Calibration Working Group will support the Duke site as needed in this effort.

The addition of new clinical collaborators, such as those studying the neuropathology of AIDS (CHARTER study) or normal aging (VETSA study) will require calibration of additional imaging sites as outlined in the Clinical Collaboration section. This will entail similar efforts as were made to extend the acquisition and correction methods from the development sites to the rest of the mBIRN sites as well as efforts to make sure that all methods are robust when applied to new clinical populations with known neuropathology. Funds have been budgeted in the Administrative Core to cover the travel expenses required to have the Project Manager collect the calibration scans at non-BIRN sites.

Subject selection

Healthy, normal adults who are willing to complete the full battery of scan sessions and have no contraindications to MRI scanning will be recruited. A minimum of 8 subjects between the ages of 18 and 40 years old will be recruited for the experiment and be studied at all participating institutions. We will complete the acquisition within 30 days to control for the potential variability in the structural data. No children will be studied because they introduce an additional confound of normal developmental changes that must also be studied later.

Inclusion criteria are: healthy adults aged 18-40 (by self-reported history), no contraindications to MRI scanning and ability to schedule trips to the 8 sites within the one month period, without loss of salary (mBIRN cannot reimburse for lost wages). Exclusion criteria are: current or past history of major medical, neurological, or psychiatric illness, claustrophobia, history of mental illness, diabetes, cardiovascular disease, migraines, head injury or prolonged unconsciousness (> 24 hours), or history of substance abuse or alcoholism, tattoos above the shoulders, history of working with metal (e.g. shavings or fragments could be lodged in scalp or eye).

Overview of Experimental Design

After undergoing an initial assessment at one of the participating sites to determine that the subject meets all inclusion and none of the exclusion criteria, they will be recruited into the study and scheduled to travel to each of the 8 sites for participation in identical scanning sessions. The Project Manager will be responsible for the coordination and implementation of the study across the sites.

Each scan session at every site will consist of placement in the scanner for about one and a half hours during which T1 and T2 structural and DTI data will be collected. At least 24 hours later the subject will repeat the entire session to allow assessment of test-retest variability within site. After completing the full circuit of imaging sites each subject will return to the originating site for a final pair of test-retest scans again at least 24 hours apart.

D.2 Improvements in structural MR acquisition and calibration procedures

D.2.1 Correction for spatial variation in RF-coil sensitivity due to B_1 field in-homogeneity

In general, smaller coils obtain higher SNR, but have greater B_1 inhomogeneities (that is, they have greater spatial inhomogeneity of the RF coil sensitivity profile). Larger coils have more uniform sensitivity profiles but reduced SNR. On the latest generation of MR scanners, using a uniform RF coil (e.g., Body Coil) for transmit, and a head coil (or phased array surface coils) for receive, it is possible to obtain a precise estimate of the sensitivity profile of the receive coil(s) by simply dividing a head coil volume, voxel-by-voxel, by the corresponding body coil image. Once this sensitivity profile is obtained, all subsequent volumes can then be corrected by dividing each voxel's intensity by the estimated sensitivity value at that location. Note that this will not work on systems using a combined transmit & receive head coil, since the B_1 inhomogeneity will also affect the flip angle (and thus image contrast) in different parts of the volume. On such systems, the effect of spatial B_1 inhomogeneity on the resultant flip angle has to be incorporated into the MRI forward solution. We plan to characterize the receive sensitivity profile of the head coils used on standard MRI scanners, and build the appropriate normalization procedures into the B_1 inhomogeneity correction and MRI forward model.

D.2.2 Correction for spatial distortion due to B_0 field in-homogeneity

Main field (B_0) inhomogeneities can result from imperfect magnet shimming or magnetic susceptibility variations. The initial structural protocol used by mBIRN was intended to be available on any clinical scanner. As such, this sequence is limited in that it doesn't take advantage of recent advances in hardware and MR protocols. In particular, it is a relatively low bandwidth sequence, implying that distortions due to magnetic field inhomogeneities and susceptibility artifacts can be substantial. In general, there is a trade-off between high-bandwidth, low distortion, low SNR images, and low-bandwidth, high-distortion, high-SNR images.

In order to avoid this trade-off, we propose to test a high-bandwidth multi-echo FLASH sequence that minimizes distortions while maximizing SNR (this is a P41 development at MGH). In a single 8-minute scan, this sequence provides 8 high-bandwidth images, where currently we collect a single low-bandwidth one. While the individual scans can be quite noisy, the information in the ensemble is significantly greater than the previous low bandwidth FLASH scans that are the current BIRN protocol. The higher bandwidth of the multi-echo FLASH sequence, coupled with the fact that alternating echoes are collected with opposite read-out directions, results in less distortion in the images due to B_0 effects. Physiologic and bulk motion during the readout also results in fewer artifacts due both to the shorter readouts of the multi-echo sequence, and to the averaging of the readouts with alternating directions (**Figure D.1**). In addition, sophisticated image reconstruction techniques can exploit the alternating readout direction to recover parts of the image previously lost to susceptibility artifacts (Kadah, 1998, Chen, 1999, Schmithorst, 2001). While these reconstruction techniques are usually applied to EPI, they can also be adapted for use with multi-echo FLASH images. Finally, preliminary results suggest that a) the test-retest stability of image intensities is improved when using the multi-echo acquisition, probably due to its reduced sensitivity to subject motion during readout, and b) It is extremely efficient in that data are being collected almost continually throughout each TR, resulting in an increase in SNR.

In addition, T_2* effects, which decrease contrast in T_1-weighted scans, can be factored out, increasing both SNR and contrast-to-noise (CNR), as well as providing access to another biologically relevant parameter. These advantages come at the cost of the high dimensionality of the multi-echo data, raising challenging technical problems that we propose to solve by implementing the dimensionality reduction and covariance regularization procedures (P41 developments at MGH- see also Project 2.1.a for the proposed efforts to develop the grid-enabled methods for performing this analysis). Finally, the multi-echo sequence provides an efficient method of estimating proton density (PD), and T_1 and T_2* relaxation times (Fischl, in press). T_1 and PD

EYE MOTION

FLASH

FL

FLA

me

me

Relative reproducibility error

meFLA

FLA
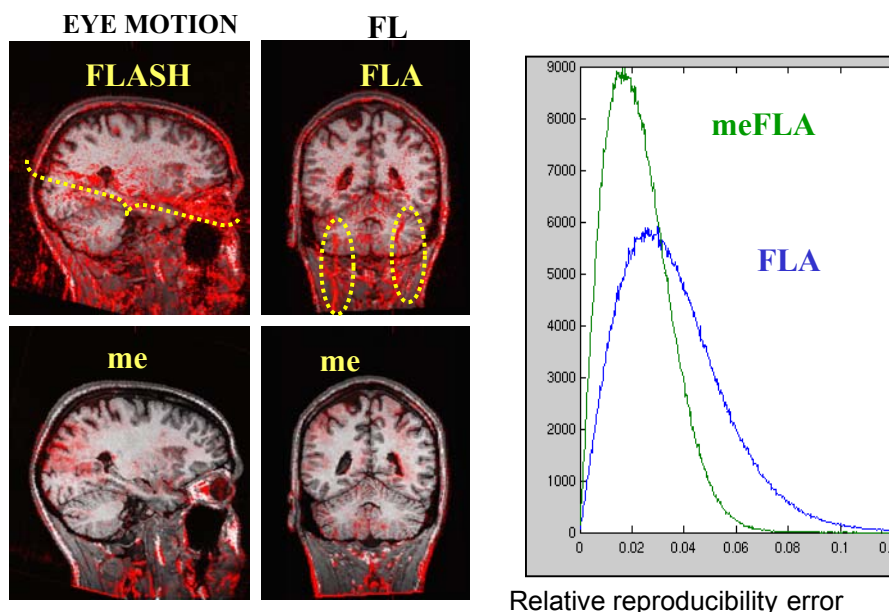
Figure D.1. Comparison of within session reproducibility of 3D FLASH30 and multi-echo 3D FLASH30 acquisitions. Red voxels indicate where the relative standard error from four acquisitions of each method obtained in a single session is greater than 8%. The histogram shows that the distribution of the magnitude of the relative errors for me FLASH (green) is shifted towards lower.

are estimated from the combination of scans with different flip angles, and T_2* is estimated from the multiple echoes of a single scan (Fischl, in press). The clinical utility of these additional tissue parameters is just beginning to be exploited as indicated by the first reports of regionally specific age related and disease related changes in cortex (Cho, 1997, Ogg, 1998, Salat, 2002, Steen, 2000).

Currently, this MR pulse sequence has been implemented at MGH for Siemens 1.5T Symphony and 3T Trio scanners. As part of this BIRN renewal, we intend to port this method to GE LX and Excite 1.5T and 3T systems (at UCSD).

D.2.3 Real-Time correction for head motion during scanning

One of the major sources of artifacts and blurring in structural images is within-scan patient motion. This has been a major impediment to the study of brain disorders and aging using anatomical imaging techniques, as patient populations almost inevitably generate lower quality images than matched controls due to within-scan motion (reviewed in Gollub, 2001). This effect is compounded for structural scans that typically take on the order of 10 minutes to collect a single high-resolution volume. Standard motion correction techniques, such as those routinely applied to functional images (e.g. Woods, 1992) do not apply in this case, as the data is collected in the spatial frequency domain. Thus, any motion during the scan results in a degradation of image quality. This is particularly problematic for automated structural analysis tools, as subject motion can cause significant underestimates in results obtained from automated procedures for computing morphometric properties such as gray matter volume (Blumenthal, 2000).

To address this problem, we are developing a method of correcting for head motion in real time during a 3D acquisition using a Cloverleaf Navigator approach (van der Kouwe & Dale, 2004). These navigators are specifically designed to enable accurate estimation of rigid-body motion during the scan. The navigators are interleaved between the partitions of a scan, enabling rotation about the three cardinal axes and translation in all three directions to be determined in a single readout of 2 ms duration. A pre-mapping of the region of k-space a small number of degrees in each direction from the initial navigator is first obtained. By comparison with this local k-space map, it is possible to determine the true rotations and translations from every subsequent navigator. A pre-scan procedure selects the optimal radius and octant angle to be used for the navigators in the map as well as the subsequent navigators. The navigators are then inserted between the phase steps of a 3D sequence to obtain a single motion corrected structural scan. The additional time required for the pre-mapping and between-partition navigators is on the order of seconds.

The application of the navigators thus consists of three steps. The first, the navigator prescan, precedes the imaging sequence. In the prescan, a separate pulse sequence is used to select the best radius and angle for the subsequent navigator mapping and imaging sequence. The next step is collecting the navigator map, which occurs during the first few seconds of the imaging sequence. The map is collected with the optimal angle and radius determined from the prescan. Subsequent motion correction navigators with the same angle and radius are interleaved between the lines or partitions of the imaging sequence. Formally, the motion correction algorithm consists of finding a path through the initial map *M*, parameterized by 3 angular perturbations (*i, j, k*), which minimizes the mean-squared difference between the current navigator N_{test} and the map *M*:

$$(1) \qquad E_{test,i,j,k} = \sqrt{\left(\left| \mathbf{N}_{test} \right| - \left| \mathbf{M}_{i,j,k} \right| \right)^T \left(\left| \mathbf{N}_{test} \right| - \left| \mathbf{M}_{i,j,k} \right| \right)},$$

where $M_{i,j,k}$ is a path through the navigator map perturbed by the angles $i\Delta\theta$, $j\Delta\theta$ and $k\Delta\theta$ about the R (right), A (anterior) and S (superior) axes respectively. The i, j and k that minimize $E_{test,i,j,k}$ then give the rotations that best match current navigator and the map.

The translations are obtained from the phase difference between the incoming navigator and the best match in the map. The following equation is solved for the translations in the x, y and z directions:

(2) $\Delta\phi(n, \Delta x, \Delta y, \Delta z) = e^{-2\pi(\Delta x.x_n + \Delta y.y_n + \Delta z.z_n)}$,

where Δx, Δy and Δz represent the translations in the x, y and z directions respectively, and x_n, y_n, and z_n represent the coordinates in k-space of the nth navigator sample. The value of $\Delta\phi$ is given by the difference in phase between the incoming (translated) navigator and the matching reference in the rotation map:

(3) $\Delta\bar{\phi} = \angle\overline{N}_{translated} - \angle\overline{N}_{reference}$

Corrections to the angles will be made in real-time by adapting the rotation angle of the gradients. Translations correspond to phase errors in the k-space representation of the image, and as such do not necessarily need to be corrected in real time. The phase correction can be made just before image reconstruction, in accordance with the equation above.

A prototype version of this method has been implemented at MGH for Siemens 1.5T Symphony (VB21b) scanners, with a representative result shown in Fig. D.2. As part of this BIRN renewal, we intend to port this method to other scanner platforms, including GE Excite 1.5T and 3T (at UCSD).
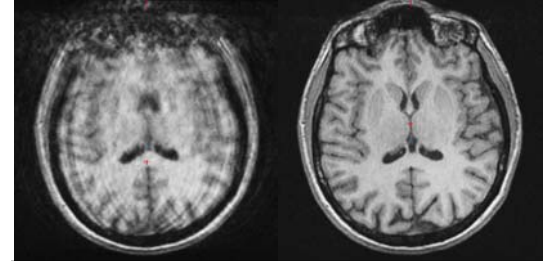
Figure D.2. No motion correction (left). Real-time motion correction (right).

D.2.4 Correction for gradient distortions, now extended to new vendors and scanner models

In Section C. 1 we clearly demonstrated that the correction of the gradient non-linearities at 1.5T improved the cross-site reproducibility of T1 weighted images. These non-linearities are even more pronounced at higher field strengths and for whole body imaging. Therefore as part of this BIRN renewal, we plan to implement and test the correction procedure on all the scanners represented at the participating sites, and streamline the process for extending the methods to additional scanner models used by our clinical collaborators. In order to generalize this technique to other scanners, and to validate the un-warping procedure, we intend to use the same specially designed cylindrical phantom (250mm diameter x 220mm) constructed from plastic plates with 10mm diameter fluid filled spherical depressions spaced on an even 20 +/- 0.05mm grid to characterize the distortion pattern due to gradient nonlinearities on each MRI system. This phantom will be scanned using a 3D FLASH/SPGR sequence (TR=20ms, flip angle=5°, TE=min) with a resolution of 1x1x1mm. An iterative, least squares algorithm will be used to optimize the match between the observed and predicted 3D MRI data. The z-component of the magnetic field pattern generated by each gradient coil can be written in terms of its Fourier-Legendre basis:

(4) $B_z\left(r,\theta,\phi\right) = \sum_{n=0}^{\infty}\sum_{m=0}^{n}\left(\frac{r}{R_0}\right)^n P_{nm}\left(\cos\theta\right)\left[A_{nm}\cos\left(m\phi\right) + B_{nm}\sin\left(m\phi\right)\right],$

where $P_{nm}(z)$ denotes the associated Legendre polynomial, and A_{nm} and B_{nm} are the unknown coefficients we wish to solve for (Press, 1994). The predicted distortion at each point in space can then be calculated directly from the deviation of B_z from the ideal, linear function of the corresponding coordinate axis. The image intensity-scaling factor is further given by the determinant of the Jacobian matrix of the map function. Note that in addition to solving for the spherical harmonic coefficients, we will also fit for an unknown rigid-body transformation of the phantom, to allow for small errors in positioning and alignment of the phantom with the isocenter and coordinate axes of the magnet.

The implementation of these methods will be performed at UCSD and MGH. Once thoroughly validated as part of the mBIRN testbed, we intend to make the software available to the research community, both as a stand-alone program for un-warping DICOM images, and through the Freesurfer package (see Project 2).

D.2.5 Calibration of T_1, T_2 acquisitions across sites, vendors, field strengths, protocols

Investigators at Duke University will create a multi-contrast calibration data set of subjects who are known to have the characteristic vascular brain lesions associated with aging and depression. They will recruit and scan elderly subjects who are known to have vascular lesions through the imaging assessment they receive in the Duke Conte Center for the Neuroscience of Depression. The subjects will be scanned twice within six months of their assessment scan on two 1.5T MRI systems of different vendors (Siemens, GE), a 3T Siemens system

and a 4T GE system. This data set will be processed using the best available segmentation algorithms available through work in Aim 2 of this application to identify brain tissue (gray, white and CSF) as well as the lesions (see preliminary data for an example). Experts at Duke will examine the results, identify and edit the lesion images to produce a validated reference set. Because it is a reference set that will be used for testing of algorithms it is only necessary to perform this extensive evaluation on a few subjects. Thus we plan on scanning and validating two subjects per year for this effort, for a total of sixteen scans per year.

The initial protocol for this effort is to acquire T_1 weighted 3D data at two flip angles (a subset of the original BIRN scan) plus proton density and T_2 weighted data and FLAIR data. As an example, on a 1.5GE Signa system the pulse sequence parameters would be as follows:

1. 3D, SPGR, axial, 25cm FOV, 1.5mm slice, gap=0, Tr=20ms, Te=minimum full echo, flip angle=30 degrees,192(phase)x256(frequency)x128 (slice) matrix, full bandwidth==25 KHz, time: 8.2 minutes
2. 3D, SPGR, axial, 25cm FOV, 1.5mm slice, gap=0, Tr=20ms, Te=minimum full echo, flip angle=5 degrees,192(phase)x256(frequency)x128 (slice) matrix, full bandwidth==25 KHz, time: 8.2 minutes
3. 2D, FLAIR, axial, 25cm FOV, 2mm slice, gap=0 interleave, Tr=9000, TI=2250, Te=100, ETL(echo-train-length)=14 (automatically chosen for GE), 256(phase)x256(frequency), full bandwidth=32KHz, time: 14.5 minutes for 75 slices (4 acquisitions).
4. 2D, PD-weighted, axial, 25cm FOV, 2mm slice, gap=0 interleave, Tr=4000, Te=17, ETL(echo-train-length)=8, 256(phase)x256(frequency), full bandwidth=32KHz, time: 6.3 minutes for 75 slices (3 acquisitions).
5. 2D, T2-weighted, axial, 25cm FOV, 2mm slice, gap=0 interleave, Tr=4000, Te=100, ETL(echo-train-length)=8, 256(phase)x256(frequency), full bandwidth=32KHz, time: 6.3 minutes for 75 slices (3 acquisitions).

The pulse sequences will be tailored to the differences between systems and to adjust for RF power absorption limits at the higher magnetic fields.

D.2.6 Calibration and modeling of healthy and lesion brain tissue contrast (T_1 and T_2) as a function of field strength, scanner model, and pulse sequence

Investigators at Duke University will develop a set of images in which model lesions have been placed that conform to the characteristics of vascular lesions that will be evaluated from existing data sets of such lesions and the work described in D.1.5. This set of images can then be used to model a variety of lesion detection tasks using the automated tools that will be provided by work in Project 2. The modeling will be done by using normal elderly subject data that has been assessed by experts at Duke to not contain detectable lesions. This normal data is already available from subjects in the Duke Conte Center for the Neuroscience of Depression. The addition of lesions will proceed as described in the more complicated method we have developed for the time change appearance of simulated MS lesions (Gerig, 2000). An example of the simulated MS lesions is shown in **Figure D.3**. While this previous work focused on the time series appearance of the lesions, the present work will focus more on reproducing the range of intensities, locations and "blobby" appearance of the vascular lesions.

1-D evolution
a

Slice of 4-D MRI
b

0 [color scale] 11
c
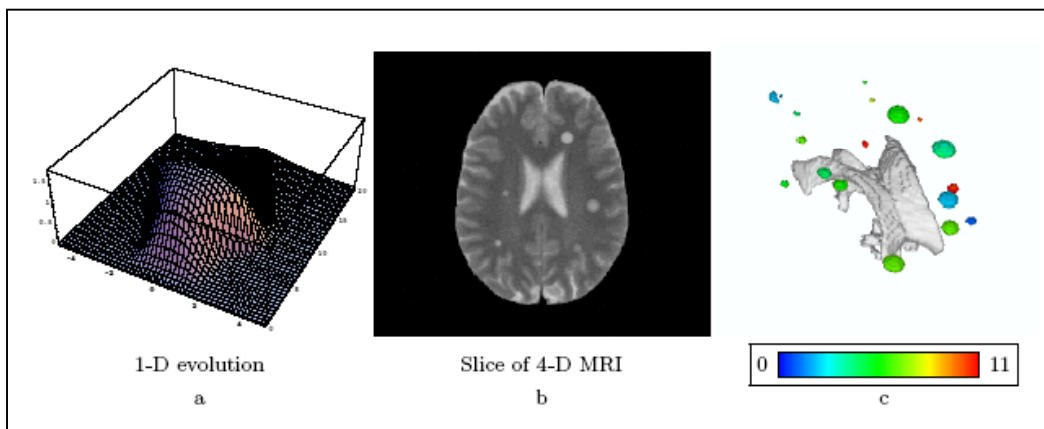
D.3 Development and validation of acquisition and calibration procedures for DTI

In this proposal, we will concentrate on two types of efforts important for calibration and optimization of DTI imaging. First, we will investigate sources of variability that are known to affect DTI results. Second, we will perform initial measurements of intra and inter-institutional reproducibility. These

results will provide crucial information for the optimization of the technique to reduce cross-platform variability.

For the characterization of the sources of variability, we will study 1) image distortion, 2) imaging parameters, and 3) k-space encoding schemes. As mentioned in the Background section (B-2), image distortion due to B_0-inhomogeneity and Eddy currents could be a significant source of variation in DTI, which currently relies on single-shot imaging. While this problem could be mitigated by improvement in hardware (e.g. shimming) or data acquisition schemes (e.g. parallel imaging), post-processing correction could significantly reduce the inter-measurement variability. The Duke and UCSD sites will investigate the amount of variability (intra-site) and improvement by post-processing distortion correction based on phase mapping and time-domain reconstruction. The JHU site will investigate effects of basic imaging parameters on DTI results. The purpose of the study is to identify imaging parameters that may have significant impact on inter-site mismatch of DTI results. These include signal-to-noise, choice of b-values, the number of gradient orientations, image resolution, and echo time.

D.3.1 Characterization of the base acquisition sequence dependence in the presence of field inhomogeneity and development of reliable correction methods

In contrast to traditional anatomy-based MRI in which only the conventional imaging sequences are used, DTI often utilize fast imaging sequence to reduce the otherwise lengthy acquisition time. They are therefore susceptible to the common vulnerabilities of fast imaging sequence to the Bo inhomogeneity, imperfect gradient waveform fidelity, and eddy currents induced by rapid gradient switching. Moreover, they are sensitive to additional artifacts unique to DTI acquisition, such as diffusion-weighting-direction dependent image distortions for the same image location. Although methods to address and correct the effect of Bo and gradient field inhomogeneity have been proposed and effectiveness demonstrated, related direction-dependent distortions from the use of multi-directional diffusion-weighting gradients in DTI acquisitions have not been systematically investigated and developed. As a result, there often exist significant mismatches among diffusion-weighted images along different weighting directions, leading to gross inaccuracy in image registration among the diffusion weighted images and with the high-resolution anatomy.

From the discussion in the preliminary results section on distortion correction, long readout time used for fast DTI and q-space imaging techniques would lead to large phase errors. These phase errors are the main cause of geometric distortions. In general, there are two types of geometric distortions: 1) distortion induced by inhomogeneous sample (e.g. human head), 2) distortion induced by the imperfect gradient fields to achieve weighting at different directions. Distortion type 1 is field dependent, that is, becoming worse at high field scanners common in the BIRN project. Distortion type 2 is gradient system dependent, and can be very severe at high weighting strength. For EPI-based acquisition, the distortions tend to displace pixels geometrically, while in spiral-based acquisition, the distortions are mainly manifested as spatial blur. Specifically designed acquisition methods, algorithms, and procedures will be required to achieve reliable DTI images.

Since the key to correct the distortions relies heavily on accurate information about the magnetic field, a distortion-free field map is needed. Our first task here is to evaluate the adequacy of the available field mapping methods to justify the need to develop a better method for a distortion-free magnetic field map. We start by examining the source and magnitude of the spatial distortion in a conventional scan where the k-space is filled one line a time from each excitation. If the readout time is denoted t' ranging from $-T_{ro}/2$ to $T_{ro}/2$, then the MR signal at time t after the excitation is given by:

$$S(t) = \int_x \int_y m(x,y) \cdot e^{-i2\pi(k_x(t')\cdot x + k_y(t')\cdot y + \Delta B_o \cdot t)} \, dxdy = \int_x \int_y m(x,y) \cdot e^{-i\gamma(G_x \cdot x \cdot t' + G_y \cdot T_p \cdot y + \Delta B_o \cdot (t' + TE))} \, dxdy$$

$$= \int_x \int_y m(x,y) \cdot e^{-i\gamma(G_x t'(x + \frac{\Delta B_o}{G_x}) + G_y \cdot T_p \cdot y + \Delta B_o \cdot TE)} \, dxdy = \int_x \int_y m(x,y) \cdot e^{-i\gamma(G_x t'(x + \frac{\Delta B_o}{G_x}) + G_y \cdot T_p \cdot y)} \cdot e^{-i\gamma \cdot \Delta B_o \cdot TE} \, dxdy$$
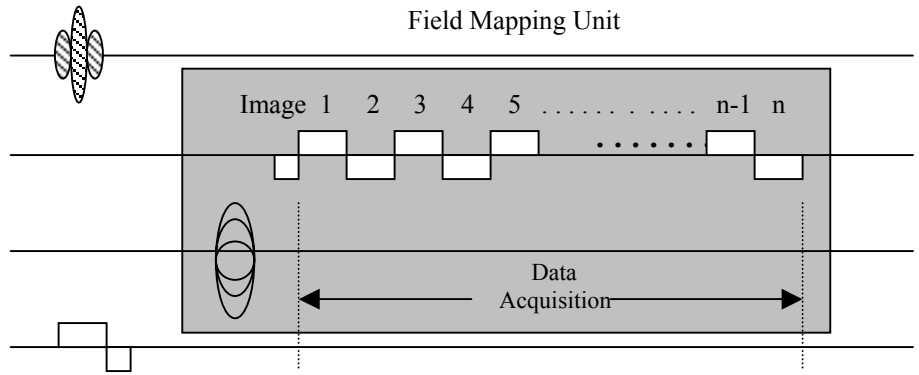
where $m(x,y)$ is the true image, k_x and k_y the k-space trajectory, G_x and G_y the strength of the frequency and phase encoding gradients, ΔBo is the field variation map (referred to as field map from now on), TE the echo time, T_p the duration of the phase-encoding gradient and T_{ro} the entire readout time. If we examine the impulse response function of this system (i.e., let $m(x,y)$ be $\delta(x_o, y_o)$), the MR signal becomes

$$S(t) = e^{-i\gamma(G_x \cdot t'(x_o + \frac{\Delta B_o}{G_x}) + G_y \cdot T_p \cdot y_o)} \cdot e^{-i\gamma \cdot \Delta B_o \cdot TE}$$

It is demonstrated that the distortion will occur along the direction of readout inversely proportional to the readout gradient strength. For a typical anatomical scan with FOV of 24 cm, matrix of 256^2, and sampling bandwidth of 16 kHz, the readout gradient strength is 0.156 G/cm. For a susceptibility-induced field change of 1 ppm at 4T (often times the field change can get up to several ppm near air/tissue interface), the corresponding spatial shift will be ~2.6 mm corresponding to ~3 pixel shifts. Thus the field maps collected

using conventional high resolution scans also may not be accurate.

For EPI scans where the phase encoding steps are completed within one excitation, the MR signal from – $T_{ro}/2$ and $T_{ro}/2$ can be analyzed similarly as the conventional scans for each line in the k_x direction. However, the distortions along k_y direction are different since the sampling frequency is much lower, actually (N + $2*N_{ramp}$) times lower where N is the matrix size and N_{ramp} the points on the ramp for EPI scans. So if we consider a typical EPI setting at FOV of 24 cm, matrix of 64^2, and sampling bandwidth of 125 kHz or higher, the minimum readout gradient strength is 1.223 G/cm. For the same 1 ppm field change at 4T, the corresponding spatial shift is 0.3 mm or less than $1/10^{th}$ of a pixel. This distortion can actually be neglected. However, the distortion along the phase encoding direction amounts to ~27.6 mm if ten points are collected on the ramp. This

Fig. D.4 Pulse sequence to acquire distortion-free field maps

indicates that the field map generated by fast imaging methods such as EPI would be severely distorted itself, and would therefore be of little value for distortion correction purposes.

A method that can generate field maps without contamination from the inhomogeneity of the magnetic field is desired. In order to do this, we plan to use conventional phase encoding combined with EPI readout trains to collect multiple images continuously at progressing echo times (Song, 1994; Posse, 1994). **Figure D.4** illustrates the imaging principle of this technique showing that each image is composed from the data taken from the same short segment at the free induction decay (FID). The very short readout time for each individual image will lead to minimal distortion, although it is worth noting that the intra-voxel dephasing term is still proportional to the TE. This intra-voxel dephasing term, however, does not affect the collection of the magnetic field map since it is based on the phase maps. The distortion-free field map can then be used to obtain accurate information of the magnetic field.

Given the unique acquisition procedure of DTI and q-space imaging, i.e., the use of multi-directional diffusion-weighted gradients, the distortion characteristics are dependent on the different diffusion weighting directions. To provide specific and tailored correction for different diffusion-weighting directions, we propose the following approach:

1. Gradient imperfections will be measured by acquiring distortion-free magnetic field maps (developed above) in phantoms at all directions within a spin-echo sequence identical to the DTI acquisitions that will be carried out in human subjects. Such a calibration process should be performed across all BIRN sites for all scanners, using the identical DTI sequences that will be used for human subjects.

2. A subject-specific distortion-free magnetic field map will be collected using the acquisition techniques developed above but based on a spin-echo implementation identical to the DTI imaging sequence.

3. A DTI imaging sequence, EPI or spiral, will be carried out in human subjects to obtain preliminary base images and diffusion-weighted images at different directions.

The subject-specific field map will be used to correct for Bo inhomogeneity induced spatial distortions, and gradient-direction-specific field maps will be used to correct for the discrepant distortions across different diffusion weighting directions. The same subject will be scanned multiple times and results compared with and without field mapping correction for distortion.

Distortion reduction through time domain image reconstruction

A variation of the approach described above for correcting for distortions due to combine EPI images collected using opposite phase-encoding directions (and thus opposite spatial distortion -- see **Figure D.5**). This ensures invertibility, even in regions where the B_0 spatial gradient is large enough to "fold" the image onto itself in one of the phase-encoding directions. Such cases would result in a singular problem with the conventional approaches to B_0 correction.

More precisely, a gradient echo (GRE) or spin echo (SE) pulse sequence can be represented as a series of excitations and signal measurements (readouts), the measured signal $y_q(t)$ following the q-th RF excitation is

expressed as follows:

$$\text{GRE: } y_q(t) = \sum_{\mathbf{R}} \iiint_{\mathbf{r} \in \mathbf{R}} x(\mathbf{r}) e^{-i\mathbf{K}_q(t)\cdot\mathbf{r}} e^{-i\Delta\omega(\mathbf{r})t} d\mathbf{r}, \text{ SE: } y_q(t) = \sum_{\mathbf{R}} \iiint_{\mathbf{r} \in \mathbf{R}} x(\mathbf{r}) e^{-i\mathbf{K}_q(t)\cdot\mathbf{r}} e^{-i\Delta\omega(\mathbf{r})(t-TE)} d\mathbf{r}$$

The variable t represents the time after excitation, TE is the echo time, and $\mathbf{K}_q$ represents the trajectory of the measurement in k-space (proportional to gradient moments). $x(\mathbf{r})$ represents the desired property of the object (transverse magnetization). $\Delta\omega(\mathbf{r})$ represents the B_0 field map, calculated from the difference in phase between two gradient echo images with different echo times. **R** represents the entire image volume and **r** represents an image voxel. The effect of T_2^* decay during the readout is assumed to be negligible.

The integral accounts for the non-constant gradients across the voxel that cause within-voxel dephasing and
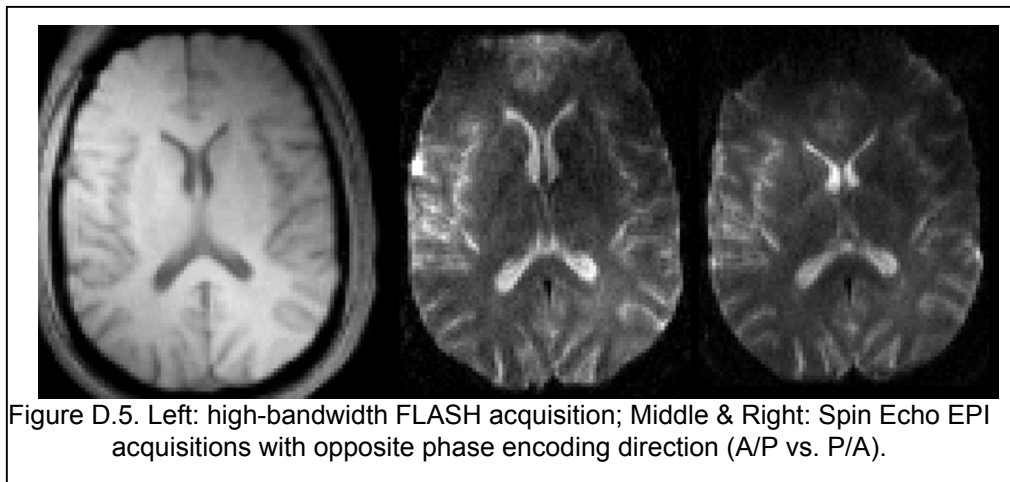

Figure D.5. Left: high-bandwidth FLASH acquisition; Middle & Right: Spin Echo EPI acquisitions with opposite phase encoding direction (A/P vs. P/A).

signal dropout. Assuming that $x(\mathbf{r})$ is uniform within each voxel, it can be moved outside the integral. Assuming discrete sampling, the remaining terms can be calculated from the known B_0 field map and gradient behavior of the sequence to give a matrix $\mathbf{A}_q$ that contains the contribution to the measured signal of each voxel at each sample in time. The resulting expression $\mathbf{y}_q = \mathbf{A}_q\mathbf{x}$ can then be solved for x using a numerical optimization method. An advantage of this approach is that it yields a least-squares optimal solution to the image reconstruction/correction problem.

D.3.2 Characterization and reduction of the dependence on SNR, resolution, b-value and gradient orientation

Compared to other quantitative MRI methods, DTI has several unique features in term of reproducibility. First, it is known that calculated anisotropy is sensitive to SNR (Pierpaoli. 1996). It is an important endeavor to perform inter-institutional studies to confirm the reproducibility of the SNR – DTI results relationship and provide recommendation about required SNR for data sharing and comparison. Second, the DTI result could be highly sensitive to spatial resolution. Unlike T_1, T_2, and ADC values, diffusion anisotropy is rather inhomogeneous within the white matter. Because of DTI's sensitivity to fiber orientations, small differences in spatial resolution and ROI locations may lead to significant partial volume effects. Theoretically, the higher the resolution is, the higher the anisotropy can be because of less averaging of fibers with different orientations. This is especially a problem in brain developmental studies, in which the brain size changes and the same physical resolution leads to different anatomical resolution. The third factor is b-value range. It has been demonstrated that signal attenuation due to diffusion weighting is not linear in logarithmic scale, contrary to common assumptions. Most DTI studies have been using b-value range of 600 – 1,200 s/mm^2. It is therefore important to understand the dependence of DTI results on the b-values within this range. Finally, effects of echo time have not been well characterized. In order to enhance SNR, the minimum echo time has been routinely used. However, the minimum echo time depends on scanner specifications such as available gradient strength and slew rates, as well as imaging parameters. Because water molecules in various tissue compartments are likely to have different T_2 and diffusion anisotropy, echo time difference may have impact on reproducibility in DTI results. In this project, effects of these four parameters will be systematically investigated.

D.3.2.1 Experimental design to characterize SNR effect:

1) Basic DTI protocol: FOV = 240 x 240 mm / Image matrix =128 x 128 / slice thickness = 2.5 mm (no gap) x 50 slices / AC-PC aligned axial slices / b-value = 800 s/mm^2 / gradient orientation = 15 orientation in addition to one b=0 image / TE = shortest / TR > 8s / Single-shot EPI. This protocol does not have signal averaging and each complete DTI acquisition takes approximately 3 min.

2) Measurement of SNR effect on DTI results: The 3-min DTI study will be repeated 8 times for one session of the study. These data will not be averaged in the scanner and stored separately. This session will be performed 4 times using the same subject on different days. The diffusion tensor images will be calculated using 1, 2, 4, 6, and 8-repetition datasets separately. This will provide 5 different datasets with different SNR. Improvement in SNR will be measured from the ratio between background noise and brain signal intensity of non-diffusion weighted images.

3) Analyses of SNR effect: From the 5 datasets with different SNRs, trace of the tensor (trace ADC) and fractional anisotropy (FA) will be calculated separately. The same data processing will be applied to data from the 4 different sessions. The data from different sessions will be co-registered using a rigid alignment procedure (AIR) and standard deviations of ADC and FA will be calculated in a pixel-by-pixel base. Using these datasets (5 different SNRs x 4 sessions), three questions will be asked;

a) Is there any bias in ADC or FA depending on SNR?

In this analysis, ADC and FA will be plotted as a function of SNR (the number of signal averaging) and the correlation will be studied. The analyses will be applied both in a pixel-by-pixel basis and for the entire brain. For the analyses of the entire brain, two approaches will be used. First, histograms will be created and distributions of ADC and FA will be studies as a function of SNR. Second, the white mater will be segmented by using a threshold (FA > 0.2) using the highest SNR data (8-signal averaging) and average FA values of the white matter will be calculated as a function of SNR.

b) Is SNR a dominant factor in reproducibility and if so to what extent?

In this analysis, standard deviations of the 4 different sessions will be correlated with the signal averaging. This correlation will be important information for the interpretations of subsequent analyses for image resolution, b-values, and echo times. In addition, it is also possible that, once a certain level of SNR is achieved, other factors such as patient motions are the dominant factors for reproducibility of DTI and clear correlations between the standard deviations and SNR are not observed. For this analysis, averages of the standard deviations of the entire white matter will be used.

c) Are there any brain regional differences in reproducibility and if so to what extent is it related to SNR?

Reproducibility of DTI of some brain regions may be dominated by B0-related distortion and/or patient motions rather than SNR. Spatial maps of standard deviations will be created from the 4 repeated measurements and correlation with SNR will be studied in a pixel-by-pixel basis.

D.3.2.2 Experimental design to characterize Resolution effect:

1) Basic DTI protocol and measurement: The protocol will be the same as D.3.2.1 except that image matrix will be changed to 64 x 64, 96 x 96, and 128 x 128. All matrixes will be zero-filled to obtain the final matrix size of 128 x 128. For signal averaging, the measurement will be repeated 4 times. Note that this design will include not only pure resolution effects but also other factors such as T_2* decay (point spread function), B_0 inhomogeneity, and SNR. These factors are difficult to separate and included in this resolution effect analysis. To calculate the reproducibility, 4 sessions of this measurement will be performed using the same subject at 4 different occasions.

2) Analyses of resolution effect: The data with 3 different resolutions will be first co-registered using the B_0-distortion correction scheme (D.3.1, Duke) and subsequent rigid alignment. The ADC and FA will be calculated for each data. Data from 4-different sessions will also be co-registered, from which standard deviations (reproducibility) of ADC and FA will be calculated. Using these datasets (3 different resolution x 4 sessions), two questions will be asked;

a) Is there any bias in ADC or FA depending on resolution?

In this analysis, ADC and FA will be calculated for 3 different imaging resolutions. The analyses will be applied both in a pixel-by-pixel basis for regional differences and for the entire brain. For the analyses of the entire brain, both the histogram and segmented white matter will be used as described in the previous section. If any bias is observed, the results will be compared to the previous SNR analyses to find if the bias can be explained by the SNR difference.

b) If difference in standard deviations (reproducibility) calculated from the 4 different sessions is observed for different resolutions, can it be explained by SNR difference?

We expect that reproducibility difference among different image resolutions is dominated by SNR. We test this hypothesis by observing the relationship between standard deviations and imaging resolutions and comparing the results with the previous analyses for SNR. The calculation methods will be the same as section D.3.2.1- (b) and (c).

D.3.2.3 Experimental design to characterize b-value effect:

1) Basic DTI protocol and measurement: The protocol will be the same as D.3.2.1 except that b-values will be changed to 600 s/mm^2, 1,000 s/mm^2, and 1,400 s/mm^2, which cover most of the b-values used in publications. For signal averaging, the measurement will be repeated 4 times. To calculate the reproducibility, 4 sessions of this measurement will be performed using the same subject at 4 different occasions.

2) Analyses of b-value effect: From the 3 datasets with different b-values, trace of the tensor (trace ADC) and fractional anisotropy (FA) will be calculated separately. The same data processing will be applied to data from the 4 different sessions. The data from different sessions will be co-registered using a rigid alignment procedure (AIR) and standard deviations of ADC and FA will be calculated in a pixel-by-pixel base. Using these datasets (3 different b-values x 4 sessions), two questions will be asked;
a) Is there any bias in ADC or FA depending on b-values?

In this analysis, ADC and FA will be calculated for 3 different imaging b-values. The analyses will be applied both in a pixel-by-pixel basis for regional differences and for the entire brain as described in the previous section.
b) Is there any difference in reproducibility depending on b-values?

> We expect that the b-values in this range (600 – 1,400 s/mm^2) do not have significant impact on reproducibility. We test this hypothesis by observing the relationship between standard deviations and b-values. The analyses will be applied both in a pixel-by-pixel basis for regional differences and for the entire brain as described in the previous section.

D.3.2.4 Experimental design to characterize echo-time effect:

1) Basic DTI protocol and measurement: The protocol will be the same as D.3.2.1 except that echo-time will be changed to 90, 110, and 130 ms. For signal averaging, the measurement will be repeated 4 times. This design will include not only pure echo-time effects but also SNR. To calculate the reproducibility, 4 sessions of this measurement will be performed using the same subject at 4 different occasions.

2) Analyses of echo-time effect: The data with 3 different echo times will be first co-registered using the B_0-distortion correction scheme (D.3.1, Duke) and subsequent rigid alignment. The ADC and FA will be calculated for each data. Data from 4-different sessions will also be co-registered, from which standard deviations (reproducibility) of ADC and FA will be calculated. Using these datasets (3 different echo times x 4 sessions), two questions will be asked;
a) Is there any bias in ADC or FA depending on echo time?

> In this analysis, ADC and FA will be calculated for 3 different echo times. The analyses will be applied both in a pixel-by-pixel basis for regional differences and for the entire brain as described in the resolution analysis (D.3.2.2). If any bias is observed, the results will be compared to the previous SNR analyses to find if the bias can be explained by the SNR difference. Namely, we expect increase in FA as the echo time becomes longer and SNR decreases.

b) If difference in standard deviations (reproducibility) calculated from the 4 different sessions is observed for different echo time, can it be explained by SNR difference?

> We expect that reproducibility difference among different echo times is dominated by SNR. We test this hypothesis by observing the relationship between standard deviations and echo times and comparing the results with the previous analyses for SNR. The calculation methods will be the same as section D.3.2.1- (b) and (c).

D.3.2.5 Characterization and reduction of dependence of encoding directions

High angular resolution diffusion encoding is achieved by generating gradient directions equally spaced on a sphere by tessellations of an icosahedron (Tuch 2002, 2003; Frank, 2001, 2002), as shown in Fig. D.7. The icosahedral sampling scheme has the important property that it provides a rotationally invariant sampling scheme. This is important because global rotations of the sampling strategies are rarely measured or taken into account. Non-rotationally invariant schemes can thus produce
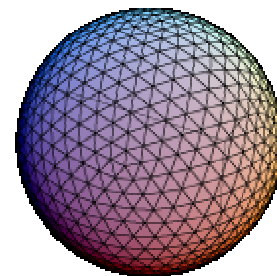

Fig. D.6 Illustration of an icosahedron sphere.

spurious anisotropy variations. The icosahedral scheme eliminates this problem to the degree that the tessellation is exact. We have developed a fast tessellation routine that requires only that the user input the tessellation level (ie, the number of times the icosahedron is recursively tessellated). The routine is written in standard ANSI C and is very short, easily transported between sites, readily incorporated into any C-based pulse programming language, as are both GE and Siemens platforms. Auxiliary code to test the tessellation program is packaged with the routine.

One of the drawbacks of the tessellation scheme, however, is that the number of samples increases dramatically with tessellation level. For example, for tessellation level 2, the number of sample directions is 42, however, the next level 3 requires sampling steps to be 162 directions. This quickly produces scan times that are infeasible. Therefore, a key question is to what degree other sampling schemes that produce approximately equal angular sampling are feasible. One such scheme is the electrostatic repulsion model (ESRM). This scheme has the advantage of being able to produce equally angle sampling for any even number of sample directions. We will perform a comparison of the tessellation scheme for three levels of tessellation 1,2, and 3, producing sampling directions of 12,42,162, with equivalent ESRM schemes (12, 42, 162 directions) and also with intermediate ESRM schemes (66 and 88 directions). Comparisons will be made by collecting data on a uniform spherical phantom with each scheme for a different number of averages (1,2,4,8) and comparing the estimates of the isotropic component of the ADC and the fractional anisotropy index (FA) for each of the schemes. This will then be repeated in normal human subjects. This test will be done repeatedly on the same subject multiple times at each site.

D.4 Analysis of multi-site calibration data

D.4.1 Data upload and de-identification procedures
Once the images are collected, they will be reconstructed locally and processed through a series of computer scripts to convert them to DICOM format and prepare them for uploading into the BIRN database. Identifying information such as name and address will be removed from the data images and replaced with a unique BIRN ID number. The date of the scan will be included so that the longitudinal nature of the data may be reconstructed. Personal information to be included will be: age (year of birth), handedness, gender, medical history (which will be none for this group as they are healthy controls), current medications (also none), and the subject category (in this case, healthy and without an Axis I diagnosis in DSM-IV). Authorization to share this data within the BIRN consortium is documented in the Informed Consent form.

D.4.2 Assessment of accuracy of image acquisition and calibration methods
The performance of the proposed acquisition and correction procedures will be evaluated using three general metrics: 1) degree of residual spatial distortion; 2) variance of image intensities across sessions and sites; 3) variability of analysis results (e.g., tissue segmentation, using the methods described in Project 2) across sessions and sites. This will be used to validate and optimize the proposed methods.
Spatial distortion will be assessed using both mechanical phantoms (as described in Section C.1) and human volunteers. Since the geometry of the phantom is known (to a precision of 0.1mm), an exact estimate of 3-D spatial displacement can be obtained by measuring the position of each lattice point in the voxel matrix relative to its actual position (after fitting for the position and orientation of the phantom in scanner coordinates). Note, however, that some sources of spatial distortion, such as those caused by B_0 inhomogeneities, depend on the object being imaged, and thus cannot be fully characterized using a mechanical phantom. We will therefore further assess the performance of the acquisition and correction procedures by estimating apparent non-rigid spatial displacements in human volunteers across sessions and scanner sites. Data from the same subject across sessions and sites will first be compared qualitatively, after fitting for rigid-body alignment of the brain, using visual blink-comparison of corresponding slices through the registered volumes. Further, non-linear registration methods (Fox, 1997; see also Project 2) to obtain estimates of local spatial displacements and compression/expansion.
Reproducibility of image intensity information will be assessed by calculating the voxelwise variance in image intensity, after spatial co-registration and correcting for relative overall image intensity scaling, across sessions within- and across sites. Similar analyses will be performed on the parametric images computed from the DTI data (e.g., ADC and FA maps). The data will be put into an ANOVA to estimate the relative contribution of variance from subject, site, and session number.
Finally, the effect of the acquisition and correction procedures on morphometric measures will be assessed by comparing the results of the segmentation and quantification procedures described in Project 2 across

sessions and sites. Specifically, data from each subject and session will be analyzed using the Freesurfer software to obtain estimates of cortical thickness and segmentation of sub-cortical structures. The consistency of segmentation results across sessions will be assessed using Dice/Jaccard (Harper, 1999) similarity metrics and intraclass correlation coefficients for each structure.

D.5 Timeline

Stages	Project 1: Calibration Tasks	Year 1	Year 2	Year 3	Year 4	Year 5
I	**Structural MRI Calibration** B_1 inhomogeneity correction B_0 inhomogeneity correction Online motion correction Gradient distortion (new sites, 1.5T and 3T) Calibration of FSE (PD, T_2, FLAIR) Healthy and lesion brain tissue modeling	░░	░░	░░		
	Diffusion MRI Calibration Base sequences effects (EPI & Spiral) SNR, spatial resolution and b-factor effects Gradient encoding direction effects	░░	░░	░░		
	Plan calibration for additional imaging methods	░░	░░	░░		
II	**Extension to additional imaging methods** Methods defined during Stage I **Distribution and support of Stage I methods**				░░	░░

REFERENCES

Basser, P. J., J. Mattiello, et al. (1994). "Estimation of the effective self-diffusion tensor from the NMR spin echo." J Magn Reson B **103**(3): 247-54.

Basser, P. J., J. M. Mattiello, et al. (1994). "MR diffusion tensor spectroscopy and imaging." Biophysical J. **66**: 259-267.

Blumenthal, J., H. Liu, et al. (2000). Motion artifact in magnetic resonance imaging: Implications for automated analysis of clinical samples. Human Brain Mapping, San Antonio.

Chen, N.-k. and A. M. Wyrwicz (1999). "Correction for EPI Distortions Using Multi-Echo Gradient-Echo Imaging." Magnetic Resonance in Medicine, **41**: 1206-1213.

Cho, S., D. Jones, et al. (1997). "Establishing norms for age-related changes in proton T1 of human brain tissue in vivo." Magnetic Resonance Imaging **15**(10): 1133-43.

Fischl, B, DH Salat, AJW van der Kouwe, N Makris, F Ségonne, A M Dale, Sequence-Independent Segmentation of Magnetic Resonance Images, Neuroimage (2004, in Press Fox, N. C. and P. A. Freeborough (1997). "Brain atrophy progression measured from registered serial MRI: validation and application to Alzheimer's disease." J Magn Reson Imaging **7**(6): 1069-75.

Frank, L. M., E. N. Brown, et al. (2000). "Trajectory encoding in the hippocampus and entorhinal cortex." Neuron **27**(1): 169-78.

Frank, L. M., E. N. Brown, et al. (2001). "A comparison of the firing properties of putative excitatory and inhibitory neurons from CA1 and the entorhinal cortex." J Neurophysiol **86**(4): 2029-40.

Gerig, G., D. Welti, et al. (2000). "Exploring the discrimination power of the time domain for segmentation and characterization of active lesions in serial MR data." Med Image Anal **4**(1): 31-42.

Gollub, R. and F. Shellock (2001). Claustrophobia, anxiety, and emotional distress in the magnetic resonance

environment. Magnetic Resonance Procedures: Health Effects and Safety. F. G. Shellock. Boca Raton, CRC Press**:** 197-216.

Greve, D., A. van der Kouwe, et al. (2003). Weighting of multiple gradient echo images to improve detection of fmri activation. Human Brain Mapping, New York.

Haacke, E. M. and G. W. Lenz (1987). "Improving MR Image Quality in the Presence of Motion by Using Rephasing Gradients." American Journal of Roentgenology **148**(6): 1251-8,.

Harper, D., Ed. (1999). Numerical Palaeobiology, John Wiley & Sons.

Jezzard, P. and R. S. Balaban (1995). "Correction for geometric distortion in echo planar images from B0 field variations." Magn Reson Med **34**(1): 65-73.

Kadah, Y. M. and X. Hu (1998). "Algebraic Reconstruction for Magnetic Resonance Imaging Under B0 Inhomogeneity." IEEE Transactions on Medical Imaging. **17**(3).

Makris, N., A. J. Worth, et al. (1997). "Morphometry of in vivo human white matter association pathways with diffusion-weighted magnetic resonance imaging." Annals of Neurology **42**(6): 951-62.

Moseley, M. E., Y. Cohen, et al. (1990). "Diffusion-weighted MR imaging of anisotropic water diffusion in cat cerebral nervous system." Radiology **176**(2): 439-445.

Moseley, M. E., Y. Cohen, et al. (1990). "Early detection of regional cerebral ischemia in cats: comparison of diffusion and T2 weighted MRI and spectroscopy." Magn Reson Med **14**: 330-346.

Moseley, M. E., J. Kucharczyk, et al. (1990). "Diffusion-weighted MR imaging of acute stroke: correlation with T2-weighted and magnetic susceptibility-enhanced MR imaging in cats." AJNR **11**: 423-429.

Moseley, M. E., D. L. White, et al. (1990). Evaluation of vascular challenges using echo-planar MRI and an intravascular, persistant magnetic susceptibility contrast agent. Society of Magnetic Resonance in Medicine, Ninth Annual Meeting, New York, New York, USA.

Ogg, R. J. and R. G. Steen (1998). "Age-related changes in brain T1 are correlated with iron concentration." Magn Reson Med **40**(5): 749-53.

Pierpaoli, C. and P. J. Basser (1996). "Toward a quantitative assessment of diffusion anisotropy." Magn Reson Med **36**(6): 893-906.

Posse, S., C. DeCarli, et al. (1994). "Three-dimensional echo-planar MR spectroscopic imaging at short echo times in the human brain." Radiology **192**(3): 733-8.

Press, W. H., S. A. Teukolsky, et al. (1994). Numerical Recipes in C. Cambridge, Cambridge University Press.

Salat, D., B. Fischl, et al. (2002). Age-related changes in brain T1 relaxation times across the surface of the cortex. Eighth International Conference on Functional Mapping of the Human Brain, Sendai, Japan.

Schmithorst, V. J., B. J. Dardzinski, et al. (2001). "Simultaneous Correction of host and Geometric Distortion Artifacts in EPI Using a Multiecho Reference Scan." IEEE Transactions on Medical Imaging **20**(6).

Song, A. W., E. C. Wong, et al. (1994). "Echo-volume imaging." Magn Reson Med **32**(5): 668-71.

Steen, R. G., W. E. Reddick, et al. (2000). "More than meets the eye: significant regional heterogeneity in human cortical T1." Magn Reson Imaging **18**(4): 361-368.

Styner, M., C. Charles, et al. (2002). Multisite validation of image analysis methods - Assessing intra and inter site variability. SPIE MedIm.

Tuch, D.S., T.G. Reese TG, et al (2002). "High angular resolution diffusion imaging reveals intravoxel white matter fiber heterogeneity." Magn Reson Med. **48**(4):577-582.

Tuch, D.S., T.G. Reese, et al (2003). "Diffusion MRI of complex neural architecture." Neuron. **40**(5):885-895.

van der Kouwe, A. and A. Dale (2004). Rapid Real-Time Prospective Rigid Body Motion Correction During Imaging Using Clover-Leaf Navigators. ISMRM, Kyoto.

Wald, L., F. Schmitt, et al. (2001). Systematic Spatial Distortion in MRI due to Gradient Nonlinearities. International Conference on Human Brain Mapping.

Weisskoff, R. M. and T. Davis (1992). Correcting Gross Distortion on Echo Planar Images. ISMRM, Berlin.

Woods, R. P., S. R. Cherry, et al. (1992). "Rapid Automated Algorithm for Aligning and Reslicing PET Images." Journal of Computer Assisted Tomography **16**(4): 620-633.

Woods, R. P., S. T. Grafton, et al. (1998). "Automated image registration: II. Inter-subject validation of linear and nonlinear models." Journal of Computer Assisted Tomography **22**: 155-165.